NeuroImage 254 (2022) 119078

Contents lists available at ScienceDirect

NeuroImage

journal homepage: www.elsevier.com/locate/neuroimage

Functional parcellation of the hippocampus based on its layer-specific connectivity with default mode and dorsal attention networks

Gopikrishna Deshpande [a,b,c,d,e,f,g,*], Xinyu Zhao [a,h], Jennifer Robinson [a,b,c,d]

[a] AU MRI Research Center, Department of Electrical and Computer Engineering, Auburn University, 560 Devall Dr, Suite 266D, Auburn, AL 36849, USA
[b] Department of Psychological Sciences, Auburn University, Auburn, AL, USA
[c] Alabama Advanced Imaging Consortium, Birmingham, AL, USA
[d] Center for Neuroscience, Auburn University, Auburn, AL, USA
[e] Key Laboratory for Learning and Cognition, School of Psychology, Capital Normal University, Beijing, China
[f] Department of Psychiatry, National Institute of Mental Health and Neurosciences, Bangalore, India
[g] Centre for Brain Research, Indian Institute of Science, Bangalore, India
[h] Quora Inc., Mountain View, CA, USA

ARTICLE INFO

Keywords:
Resting state functional connectivity
Hippocampus
Parcellation
Layer-specific connectivity
Default mode network
Dorsal attention network
HERNET model

ABSTRACT

Recent neuroimaging evidence suggests that there might be an anterior-posterior functional differentiation of the hippocampus along the long-axis. The HERNET (hippocampal encoding/retrieval and network) model proposed an encoding/retrieval dichotomy with the anterior hippocampus more connected to the dorsal attention network (DAN) during memory encoding, and the posterior portions more connected to the default mode network (DMN) during retrieval. Evidence both for and against the HERNET model has been reported. In this study, we test the validity of the HERNET model non-invasively in humans by computing functional connectivity (FC) in layer-specific cortico-hippocampal microcircuits. This was achieved by acquiring sub-millimeter functional magnetic resonance imaging (fMRI) data during encoding/retrieval tasks at 7T. Specifically, FC between infra-granular output layers of DAN with hippocampus during encoding and FC between supra-granular input layers of DMN with hippocampus during retrieval were computed to test the predictions of the HERNET model. Our results support some predictions of the HERNET model including anterior-posterior gradient along the long axis of the hippocampus. While preferential relationships between the entire hippocampus and DAN/DMN during encoding/retrieval, respectively, were observed as predicted, anterior-posterior specificity in these network relationships could not be confirmed. The strength and clarity of evidence for/against the HERNET model were superior with layer-specific data compared to conventional volume data.

1. Introduction

The hippocampus, located in the medial temporal lobe (MTL), plays important roles in many brain functions including episodic memory and spatial navigation (Das et al., 2011; Yushkevich et al., 2010; Heckemann et al., 2011). Investigation of functional specialization within the hippocampus has received increased attention in neuroimaging. The abnormalities of the hippocampus have been identified in many neuropsychiatric disorders, including Alzheimer's disease (Lukiw, 2007; Zhou et al., 2008; Scheff and Price, 2006), major depression (Campbell and MacQueen, 2004; Stockmeier et al., 2004; Rosso et al., 2005; MacQueen and Frodl, 2011), post-traumatic stress disorder (Astur et al., 2006; Javidi and Yadollahie, 2012), and schizophrenia (Harrison, 2004; Heckers, 2001; Grace, 2012). Therefore a better understanding of the functional specialization within the hippocampus has the potential to lead to a better understanding of these disorders.

Recently, many studies have posited that there may be a functional differentiation along the long-axis of the hippocampus (Robinson et al., 2015; de Wael et al., 2018). Lepage et al. (1998) performed a meta-analysis of positron emission tomography (PET) of episodic memory and discovered an orderly functional anatomic pattern in the hippocampus. More specifically, the anterior portions were primarily activated with episodic memory encoding, whereas the posterior portions were primarily associated with episodic memory retrieval. This model is referred to as HIPER (hippocampus encoding/retrieval) model.

The HIPER model has received support from many recent studies. Spaniol et al. (2009) conducted meta-analyses of event-related fMRI studies of episodic memory and revealed an anterior-posterior gradient

* Corresponding author at: AU MRI Research Center, Department of Electrical and Computer Engineering, Auburn University, 560 Devall Dr, Suite 266D, Auburn, AL 36849, USA.
E-mail address: gopi@auburn.edu (G. Deshpande).

https://doi.org/10.1016/j.neuroimage.2022.119078.
Received 4 June 2019; Received in revised form 29 January 2022; Accepted 7 March 2022
Available online 9 March 2022.

in the hippocampal activations associated with encoding and retrieval. Nadel et al. (2013) and his colleagues compared the anterior and posterior hippocampal activations during retrieval of different types of spatial information. They found that there is a functional differentiation along the longitudinal axis of the hippocampus with the posterior hippocampus being crucial for precise spatial behavior, and the anterior hippocampus being involved in context coding. Baumann and Mattingley (2013) examined retrieval-related activity in the taxi drivers' hippocampus using fMRI data and found that taxi drivers with a small anterior hippocampus had difficulty encoding new spatial associations. Moreover, Kim (2015) conducted a meta-analysis and revealed that the encoding of sensory input involved mainly the anterior hippocampus and the external attention network, whereas retrieval engaged mainly the posterior hippocampus and the internal attention network. This model was referred to as the HERNET (hippocampal encoding/retrieval and network) model.

Memory encoding is inherently linked with external attention, whereas retrieval is intrinsically related to internal attention (Kim, 2010; Chun et al., 2011). Many studies have identified two brain networks, i.e., the dorsal attention network (DAN) and default mode network (DMN), that are closely associated with external and internal attention, respectively (Buckner et al., 2008; Corbetta and Shulman, 2002). Therefore, the HERNET model predicts that the anterior hippocampus and regions of the DAN co-activate during encoding while the posterior hippocampus and regions of the DMN co-activate during retrieval. In fact Kim (2015) meta-analysis confirms this prediction. However, evidence conflicting the HERNET model also exists. This includes meta-analyses of imaging studies which contradict Kim's findings (Schacter and Wagner, 1999), suggestions that the anterior hippocampus is activated by novelty (which is purportedly mistaken for encoding since encoding tasks typically use novel stimuli) (Kumaran and Maguire, 2006; Poppenk et al., 2008; Zweynert et al., 2011; Poppenk et al., 2010a2010b) and alternative models of functional specialization which attribute "hot" processing (emotion/motivation) to anterior hippocampus and "cold" processing (cognition) to the posterior part (Murty et al., 2011; Robinson et al., 2015; Robinson et al., 2016). Given this state of affairs, we set out to directly test the HERNET model using functional connectivity between the hippocampus and DAN/DMN regions during memory encoding and retrieval tasks. Unlike previous studies which employed voxel-level analysis from data obtained at conventional field strengths ($\lesssim$ 3T), we employed fMRI with ultra-high spatial resolution (sub-millimeter) obtained at 7T. This allowed us to investigate layer-specific microcircuits between DMN/DAN regions and the hippocampus with the hypothesis that they would provide a finer grained characterization of the connectivity between them, which in turn may provide more definitive evidence for or against the HERNET model. By fine grained characterization, we mean that the connections between the hippocampus and cortical regions in the DMN and DAN are anatomically layer-specific. Yet, the functional connectivity analyses of these circuits underlying the HIPER/HERNET models are carried at the conventional volume level, which ignores this biological reality and accepts the loss of spatial specificity. Our point is that current technology allows us to overcome this limitation by acquiring data with higher spatial specificity, which could provide evidence for or against the HIPER/HERNET model which is closer to the biological reality of these layer-specific circuits. We would also like to note that while the ventral attention network (VAN) also contributes to the allocation of attentional resources to memory processing, we restrict ourselves to the DAN since we are interested in specifically testing the HERNET model which hypothesizes only the DAN.

Previous invasive studies in animals have shown that the connections between the hippocampus and DAN/DMN primarily involve cortical layers II and V, with layer V of the higher order cortex (frontal and parietal cortices) projecting to the hippocampus, whereas layer II of higher order cortex receiving the signal back from the hippocampus (Swanson and Cowan, 1977; Thomson and Bannister, 2003). This layer-specific pathway between the hippocampus and DAN/DMN is not exclusive since pathways which originate/terminate in other layers of the cortex may also contribute to the hippocampal input or output. This is not surprising given the highly complex underlying microcircuitry and given that signals between any two brain regions can relay via multiple structures including the thalamus. However, the pathways between the hippocampus and layers II and V of the DMN/DAN seem to be the dominant ones based on prior invasive animal literature (Shepard and Grillner, 2010; Thomson and Lamy, 2007).

The present study sought to investigate the HIPER/HERNET model using the functional connectivity between the hippocampus and (1) deeper layers of DAN/DMN during an encoding task, and (2) superficial layers of DAN/DMN during a retrieval task. Specifically, we hypothesized that during a memory encoding task, clustering hippocampal voxels based on their functional connectivity with layer V of the DAN must parcellate the hippocampus in an anterior-posterior gradient along the long axis. Similarly, during a memory retrieval task, clustering hippocampal voxels based on their functional connectivity with layer II of the DMN must also show an anterior-posterior segmentation. Second, during an encoding task, the hippocampal voxels must have stronger connectivity with layer V of the DAN than with layer V of the DMN. Contrarily, during a retrieval task, the hippocampal voxels must have stronger connectivity with layer II of the DMN than with layer II of the DAN. Third, considering the directionality of signal projection, during an encoding task, layer V of the DAN must show stronger correlation with anterior hippocampal regions than with posterior hippocampal regions, whereas during retrieval task, layer II of the DMN must exhibit stronger correlation with posterior hippocampal regions than with anterior hippocampal regions. Finally, we predicted that using layer-specific data would lead to more definitive results than using conventional volume-level data while investigating the connection between the hippocampus and the DAN/DMN. All four hypotheses, based on predictions from the HERNET model, are illustrated in Fig. 1. Here it is noteworthy that although we intend to test these hypotheses using fMRI data extracted from layers II and V of DAN/DMN regions, some partial volume effects are expected for the spatial resolution of our data. Therefore, signal from layer II broadly represents those from supra-granular layers with dominant contribution from layer II. Likewise, signal from layer V broadly represents those from infra-granular layers with dominant contribution from layer V.

In order to test these hypotheses, fMRI data was acquired from healthy subjects performing memory encoding and retrieval tasks with faces, pictures of scenes and words in the 7T scanner. Ultra-high resolution anatomical data was also acquired to resolve layers in the DAN/DMN. Unsupervised clustering methods were applied, which groups objects in a data driven way without using any labels to guide the results, to parcellate the hippocampal voxels based on their connectivity with different layers in the DAN/DMN. Three clustering methods were specifically chosen, i.e., hierarchical clustering (Dasgupta and Long, 2005), ordering points to identify the clustering structure (OPTICS) (Ankerst et al., 1999), and density peak clustering (DPC) (Rodriguez and Laio, 2014), since they did not require *a priori* specification of the number of clusters. Since clustering accuracy is often lower in high dimensional feature space, a genetic algorithm (GA) based feature selection method was also employed, which is less prone to local optimum (Dy and Brodley, 2004), comparing with other existing feature selection methods, e.g., sequential forward searching (Dy and Brodley, 2004), non-linear optimization (Bradley and Mangasarian, 1998), etc.

2. Materials and methods

In this work the connectivity between the hippocampus and the DAN/DMN were investigated by clustering hippocampal voxels, in an unsupervised way, based on their connectivity with (1) layer V of DAN/DMN during an encoding task, and (2) layer II of DAN/DMN dur-

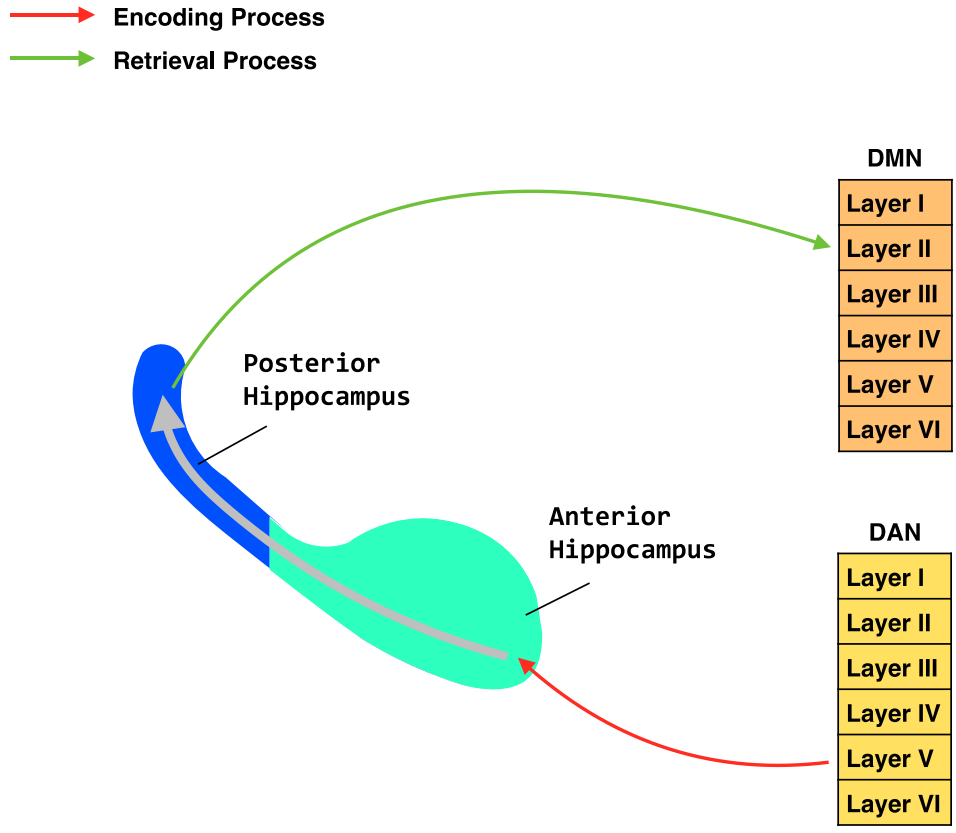

Fig. 1. Illustration of our hypotheses based on predictions from the HERNET model as well as known anatomical pathway between different layers of DAN/DMN and hippocampus.

ing a retrieval task. The identified functional clusters of the hippocampus were then compared with an anatomical anterior-posterior segmentation (Poppenk et al., 2013). The entire analysis pipeline is illustrated in Fig. 2 and will be elaborated below.

2.1. Data acquisition

Thirty-one healthy individuals (26 right-handed, 12 males, 19 females, age = 21.1 ± 1.4) were recruited for the study. The Internal Review Board (IRB) at Auburn University approved the study, subjects provided informed consent and the experimental procedures were performed in accordance with internationally accepted ethical standards. Echo-planar imaging (EPI) data were acquired on the Auburn University MRI Research Center (AUMRIRC) Siemens 7T MAGNETOM scanner outfitted with a 32-channel head coil by Nova Medical (Wilmington, MA). The sequence was optimized for the hippocampus (37 slices acquired parallel to the AC-PC line, 0.85 mm × 0.85 mm × 1.4 mm voxels, TR/TE: 3000/28 ms, 70° flip angle, base/phase resolution: 234/100, A→P phase encode direction, iPAT GRAPPA acceleration factor = 3, interleaved acquisition, 123 time points, total acquisition time 6 min). During encoding task, the participants were asked to view a series of faces, pictures of scenes and words. Each trial lasted for 30 s in which the subjects were presented 10 images of the same category for 3 s each. These trials were interspersed with a 6 s inter-trial interval. The paradigm for the retrieval task was identical to the encoding task with the exception that the subjects were provided with an MR-compatible button box to indicate, via button presses, whether they recognized the image as having seen during the encoding task or not. A whole-brain high-resolution 3D MPRAGE sequence was used to acquire anatomical data (256 slices, 0.63 mm x 0.63 mm x 0.60 mm, TR/TE: 2200/2.8, 7° flip angle, base/phase resolution 384/100%, collected in an ascending fashion, acquisition time = 14:06) for extracting different cortical layers in the DAN/DMN ROIs and for registration purposes.

2.2. Preprocessing

(a) *Hippocampal data:* Standard pre-processing steps were carried out using SPM8 (Ashburner, 2012) including brain extraction, slice timing correction, motion correction, regression of motion and physiological artifacts (using CompCor (Behzadi et al., 2007)), registration to anatomical space, and normalization to MNI standard space.
The Harvard-Oxford Structural Probability Atlas distributed with the FSL neuroimaging analysis software package (http://www.fmrib.ox.ac.uk/fsl/fslview/atlas-descriptions.html#ho) was used to define hippocampal ROIs. Our task did not explicitly involve spatial memory typically used in navigation, which is primarily associated with the right hippocampus (Burgess et al., 2002). Therefore, only the left hippocampus was considered in this study. In order to determine a conservative anatomical representation, the hippocampal ROI was thresholded at 75%. The mean probability for the voxels in the hippocampal ROIs belonging to the hippocampus (M±SD: 86.41% ± 7.10%) and the voxel centroid (MNI coordinates [−26, −18.8, −17.2]) belonging to the hippocampus was > 86% and 97.1%, respectively. The identified hippocampal ROIs are illustrated in Fig. 3 with a total volume of 1880 mm^3.

(b) *Cortical layer-specific data of the DAN/DMN*: Data extracted from the whole brain was first preprocessed using SPM8. To preserve high spatial resolution, no spatial filtering was applied. The cortical layers were then reconstructed using FreeSurfer (Fischl, 2012). Specifically, two interfaces, i.e., the cortical gray matter and the underlying white matter (white-gray interface) and the interface between the cortical gray matter and the pial surface (gray-pial interface), were automatically reconstructed from the anatomical image. Then, the cortical thickness was calculated as the average of the distance from the white-gray interface to the closest possible point on the gray-pial interface, then from that point back to the closest point on the white-gray interface again. To improve accuracy, surface smoothing and

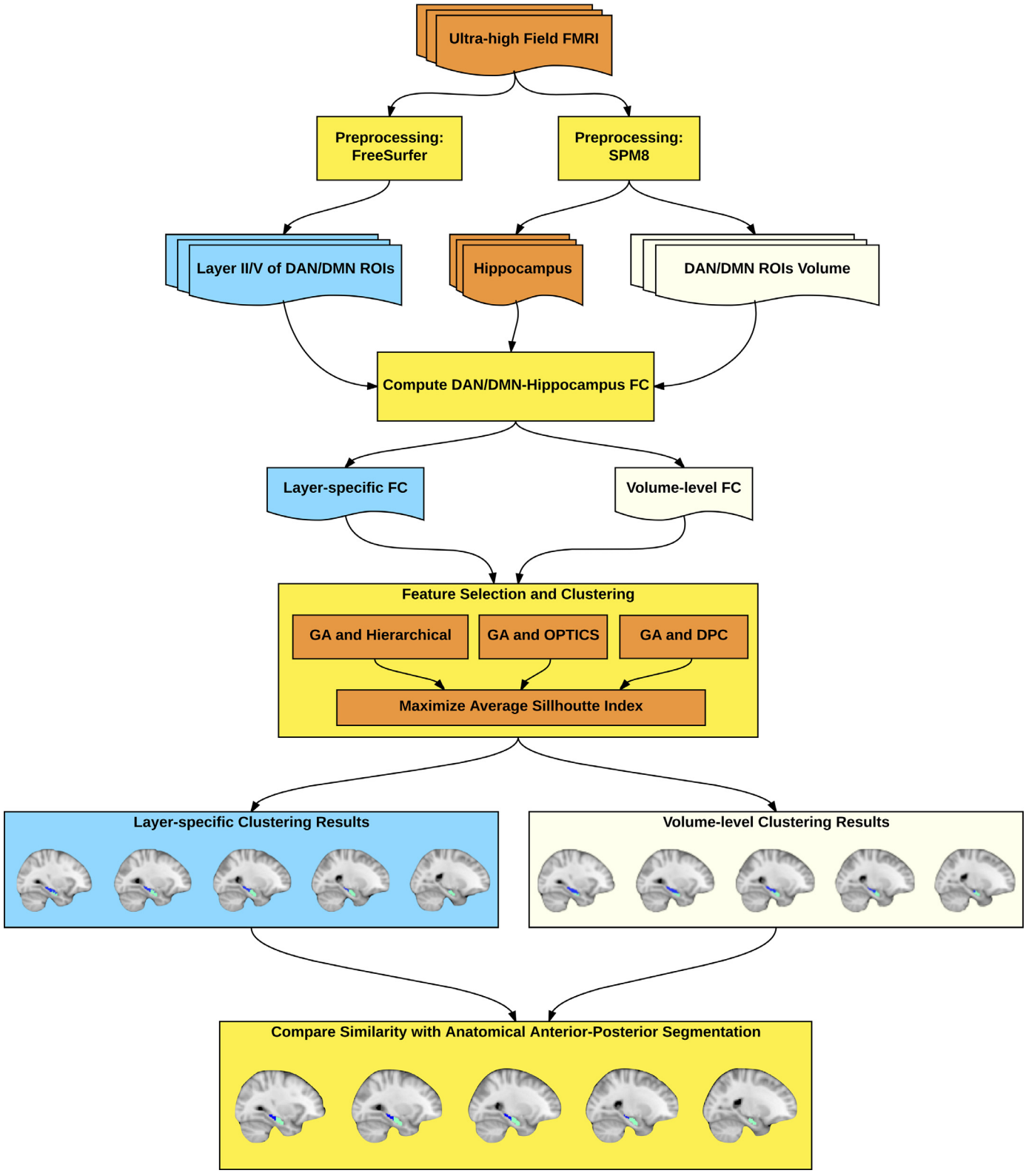

Fig. 2. Illustration of proposed analysis pipeline for investigating hippocampal parcellation based on its layer-specific connectivity with DAN/DMN ROIs. The same process was repeated for encoding and retrieval tasks, separately, as well as with conventional volume data (as opposed to layer-specific data).

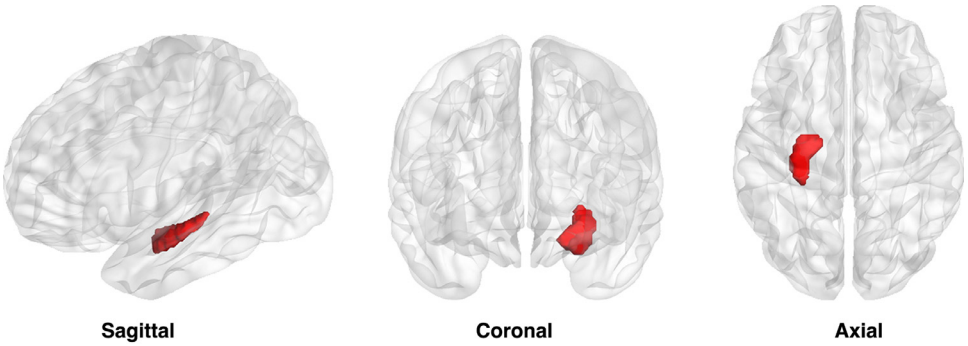

Fig. 3. Hippocampal ROI used in this study. Only the left hippocampus was considered in this study.

automatic topology correction were also applied (Dale et al., 1999; Fischl et al., 1999; Fischl and Dale, 2000; Han et al., 2006). From the cortical thickness map, six cortical layers were then reconstructed within the cortical gray matter at fixed relative distance between the white and pial surfaces determined from the cortical thickness, i.e., the first layer was located at 96% of the cortical thickness away from the white matter, the second layer at 80%, the third layer at 64%, the fourth layer at 48%, the fifth layer at 32%, and the six layer at 16% (Fig. 4). The laminar layers were derived from the anatomical image, so it was necessary to align the EPI data to these layers. A boundary-based registration method (Greve and Fischl, 2009) was employed, which aligns the EPI image to the anatomical image by maximizing the intensity gradient across white-gray interface and gray-pial interface. The entire cortical surface was automatically divided into 34 cortical ROIs in each of the individual hemispheres based on the Desikan-Killany atlas in Freesurfer (Desikan et al., 2006). The major DAN regions, i.e., frontal eye field [FEF], inferior temporal cortex [ITC], inferior frontal gyrus [IFG], and superior parietal lobe [SPL], and major DMN regions, i.e., anterior cingulate cortex [ACC], medial prefrontal cortex [mPFC], inferior parietal lobe [IPL], posterior cingulate cortex [PCC], and precuneus, were identified from those 34 ROIs, and vertices (voxels in the volume become vertices on surfaces) in layer II and layer V of these regions were then identified.

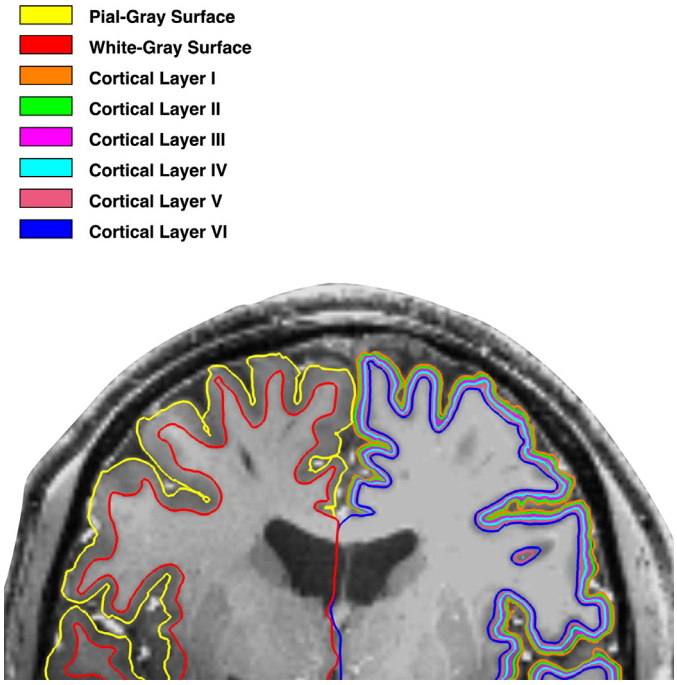

Fig. 4. Cortical layer reconstruction with FreeSurfer. Six cortical layers were reconstructed within the cortical gray matter at fixed relative distances between the white and pial surfaces.

2.3. Connectivity measures

FC measures the functional interrelationship between pairs of brain regions by estimating Pearson's correlation between time series representing those brain regions. Functional connectivity (FC) was estimated between the hippocampal voxels and (1) vertices in layer V of the DAN/DMN during the encoding task, and (2) vertices in layer II of the DAN/DMN during the retrieval task.

2.4. Layer specific clustering

The hippocampal voxels were parcellated using three clustering methods based on their FC with (1) vertices in layer V of the DAN/DMN during the encoding task, and (2) vertices in layer II of the DAN/DMN during the retrieval task. The same process was repeated on DAN and DMN volume ROIs, separately. Let $Y = \{Y_1, \cdots, Y_i, \cdots, Y_N\}$ represent a set of N objects, i.e., number of hippocampal voxels. $\boldsymbol{Y}_i = (Y_{i1}, Y_{i2}, \cdots, Y_{id}) \in \mathbb{R}^d$, where d equals to the number of FC features. Assume the N objects are separated into k clusters. Each cluster is a set of indexes from $\{1, \cdots, N\}$, and each object Y_i belongs to exactly one cluster.

(a) *Hierarchical Clustering (Agglomerative)*: As one of the most commonly used connectivity-based clustering method, the hierarchical clustering (Liao et al., 2008; Cheng et al., 2006; Dasgupta and Long, 2005) groups objects into different clusters by building a hierarchical tree structure. The procedure of this method is illustrated below:

(1) Initially, each object Y_i is assigned to a cluster with only itself in it.
(2) Distance between any two clusters is measured. Then, the closest pair of clusters are merged.
(3) Step 2–3 are repeated until all Y_i are in one big cluster.

The resulting tree structure is usually referred to as the dendrogram (Fig. 5). The root of the dendrogram represents the entire data, each leaf node represents one single object, and the height of the dendrogram represents the distance between each pair of clusters. Different data partitions can be obtained by cutting the dendrogram at different heights. Note that there are three linkage criterions, single-linkage, complete linkage, and average-linkage, which have been widely used in measuring distance between two clusters. The single linkage (Andreopoulos et al., 2008) calculates the shortest distance between two clusters, the complete linkage (Andreopoulos et al., 2008) calculates the longest distance, and the average linkage (Andreopoulos et al., 2008) calculates the mean distance. The single linkage method can handle non-elliptical shape of clusters, but can be affected by noise and outliers. The complete linkage method is less sensitive to noise and outliers but tends to break large clusters. The average linkage is a compromise between single-linkage and complete linkage methods. Thus, the average linkage method was employed in this work.

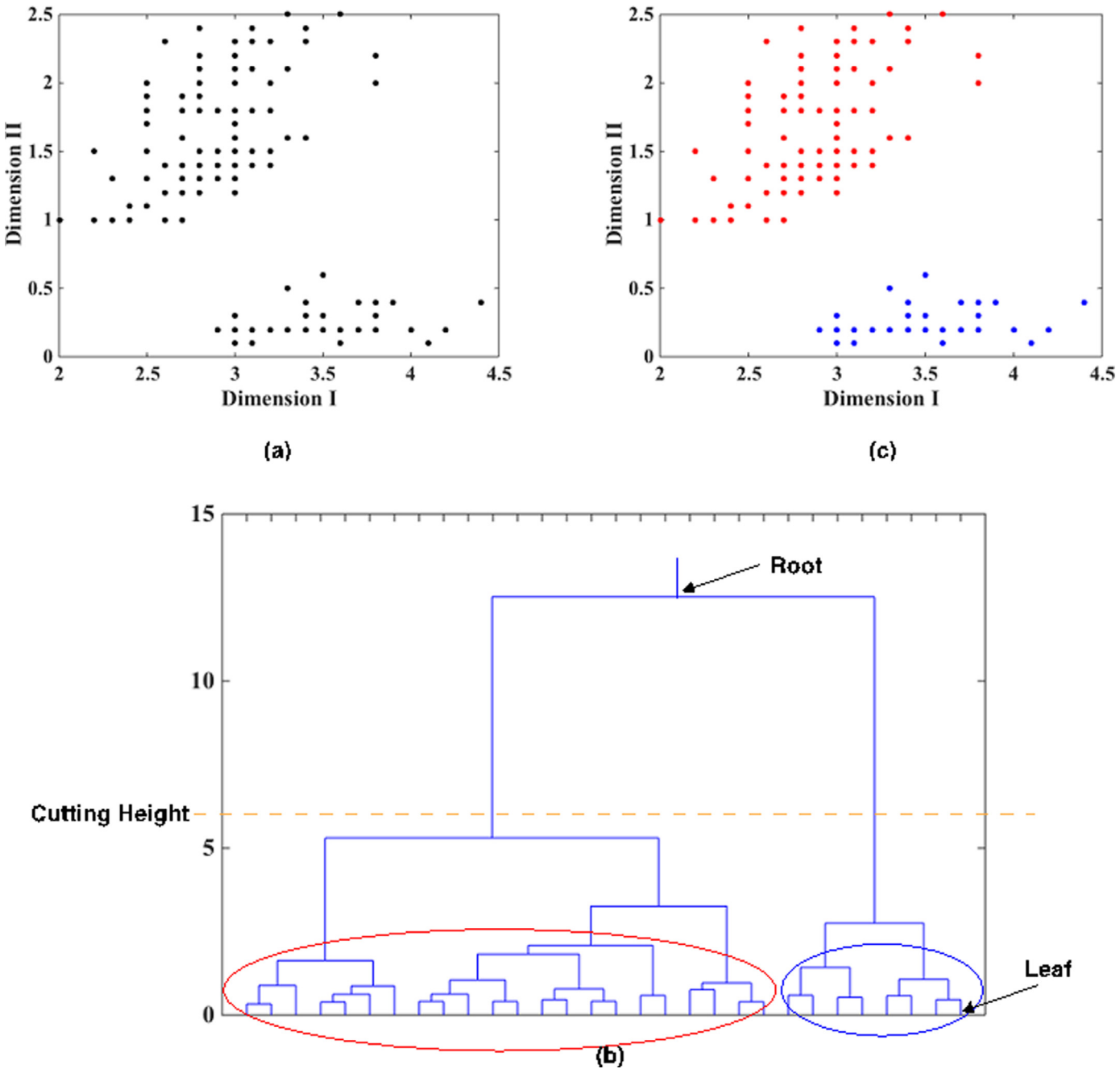

Fig. 5. Illustration of hierarchical clustering. (a) Original simulated dataset, (b) Dendrogram derived from hierarchical clustering, and (c) Clustering results obtained with a specific cutting height. Two clusters that were identified are marked with different colors.

(b) *Ordering Points to Identify the Clustering Structure*: OPTICS (Ankerst et al., 1999) is one of the most popular density-based clustering methods (Kriegel et al., 2011) Given a distance threshold (ε) and the minimum number of objects required to form a cluster ($MinPts$), objects in high-density areas are grouped together, whereas objects in sparse areas, which are required to separate clusters, are usually considered to be noise or outliers. OPTICS can discover clusters with arbitrary shapes and has the ability to identify outlier objects that do not belong to any of the clusters.

In OPTICS, two variables are computed for each object in the dataset: *core-distance* and *reachability-distance*. Let $N_\varepsilon(Y_i)$ represent the number of nearby objects within ε (called $\varepsilon - neighborhood$), and $MinPts - distance(Y_i)$ represent the distance from Y_i to its $MinPts$' neighbor. An object Y_i is a core object if at least $MinPts$ objects are found with its $\varepsilon - neighborhood$. The *core-distance* of Y_i is defined as:

$$core - dist_{\varepsilon,\ MinPts}(Y_i) = \begin{cases} Undefined\ if\ N_\varepsilon(Y_i) < MinPts \\ MinPts - distance(Y_i)\ otherwise \end{cases} \quad (1)$$

which is the smallest distance for Y_i to have $MinPts$ in its $\varepsilon - neighborhood$.

The reachability-distance of object Y_j with respect to object Y_i is defined as:

$$reachability - dist_{\varepsilon,\ MinPts}(Y_j,\ Y_i) = \begin{cases} Undefined\ if\ N_\varepsilon(Y_i) < MinPts \\ max(core - distance(Y_i),\ dist(Y_j, Y_i))\ otherwise \end{cases} \quad (2)$$

Where $dist\ (Y_j,\ Y_i)$ is the distance measure (e.g., Euclidean distance) between Y_j and Y_i. The complete procedure of OPTICS is described below:

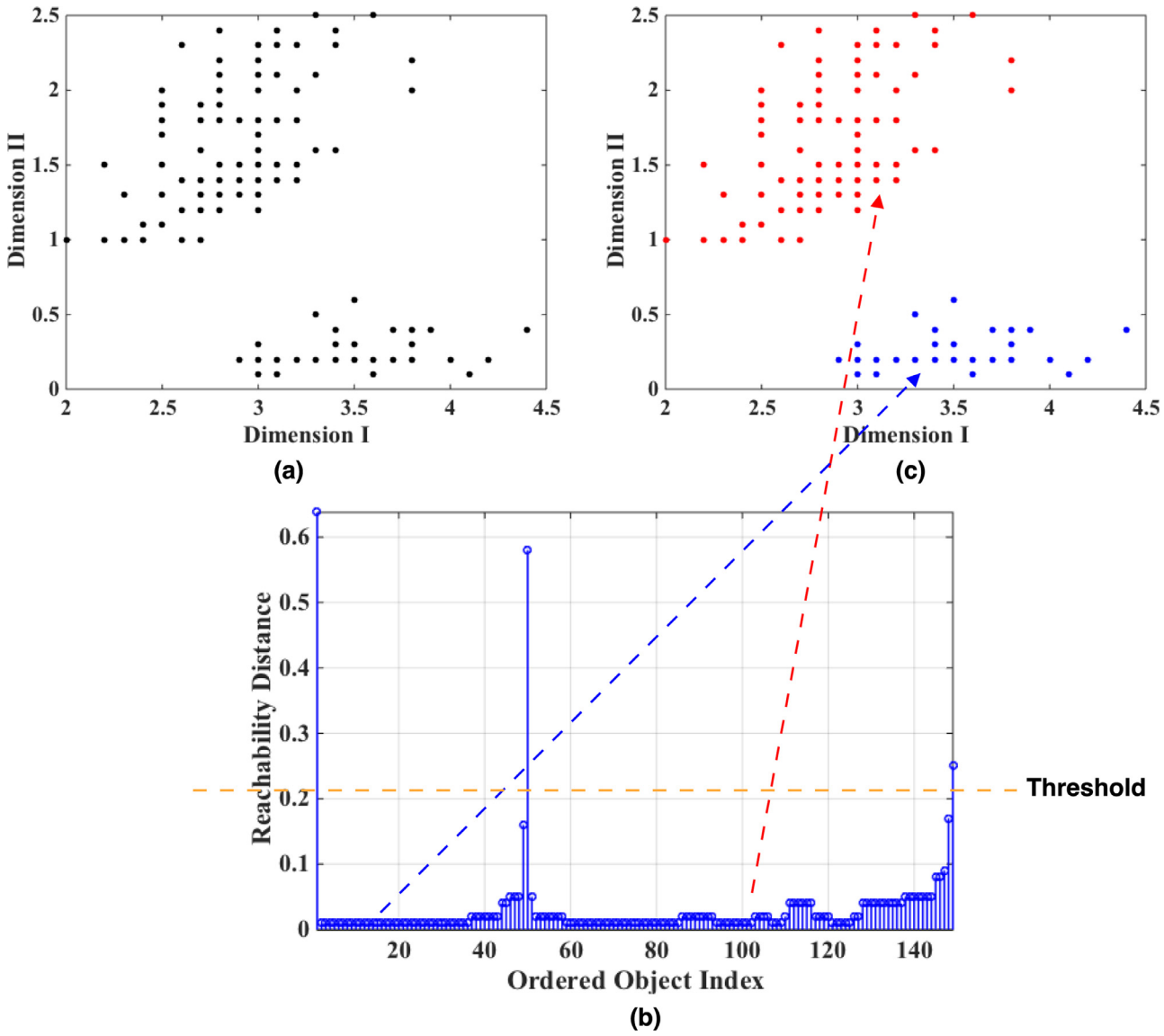

Fig. 6. Illustration of OPTICS clustering. (a) Original simulated dataset, (b) reachability plot obtained from OPTICS, and (c) clustering results. Two clusters were identified corresponding to valleys in the reachability plot.

(1) Choose one object Y_i arbitrarily.
(2) Retrieve the $\varepsilon - neighborhood$ of Y_i, determine the core-distance of Y_i, and set the reachability-distance of each object Y_j in the $\varepsilon - neighborhood$ of Y_i to undefined.
(3) If Y_i is not a core object, go to step 5. Otherwise, go to step 4.
(4) For each object Y_j in the $\varepsilon - neighborhood$ of Y_i, update its reachability-distance from Y_i and insert Y_j into an OrderSeeds list if it has not been processed yet.
(5) If the input dataset is fully consumed and the OrderSeeds list is empty, go to step 6. Otherwise, move on to the next object in the OrderSeeds list (or the input list, if the OrderSeeds list is empty) and go to step 2.
(6) Output core-distance, reachability-distance of each object, and processed order.

The data objects are plotted in the processed order together with their respective reachability-distance (called reachability plot) depicting the hierarchical structure of the clusters. Since objects belonging to a cluster have a low reachability-distance to their nearest neighbor, the clusters show up as valleys in the reachability plot (see Fig. 6). The final data partition can be obtained by using a threshold on the reachability plot.

(C) *Density Peak Clustering*: recently Rodriguez and Laio (2014) proposed a novel density-based clustering method (referred to as DPC) based on the idea that the cluster centers are characterized by a higher density than their neighbors and by a relatively large distance from objects with higher densities. Like other density-based clustering methods, e.g., OPTICS, it has ability to detect arbitrarily shaped clusters and spot outlier objects. Moreover, DPC outperforms commonly used clustering methods, e.g., k-means and hierarchical clustering, when the dataset contains complicated features such as narrow bridges between clusters, uneven-sized clusters, clusters with high overlap, etc.

For each object $\boldsymbol{Y}_i$, two quantities are computed: local density $\rho(\boldsymbol{Y}_i)$ and minimum distance with higher density $\delta(\boldsymbol{Y}_i)$. $\rho(\boldsymbol{Y}_i)$ is defined as:

$$\rho(\boldsymbol{Y}_i) = \sum_i \chi\left(dist(\boldsymbol{Y}_i, \boldsymbol{Y}_j) - \boldsymbol{d}_c\right) \tag{3}$$

where $\boldsymbol{d}_c$ is a cutoff distance, and $\chi(\boldsymbol{y})$ can be computed by,

$$\chi(\boldsymbol{y}) = \begin{cases} 1 \; if \; \boldsymbol{y} < 0 \\ 0 \; otherwise \end{cases} \tag{4}$$

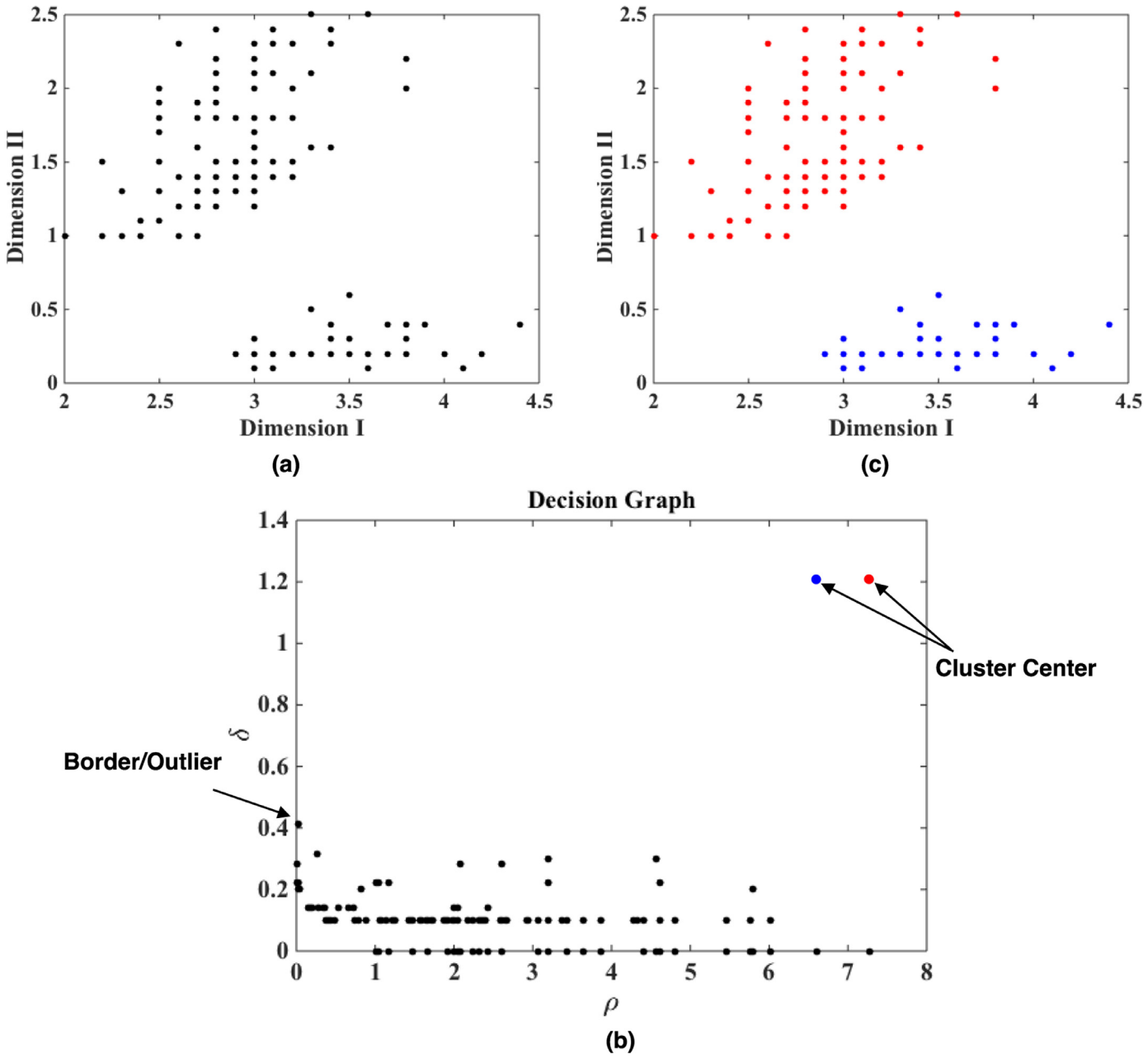

Fig. 7. Illustration of DPC clustering. (a) Original simulated dataset, (b) Plot of δ as a function of ρ for each object. Objects with larger ρ and δ are cluster centers and objects with smaller ρ, and larger δ are outliers. (c) Clustering results. Two clusters were identified corresponding to two cluster centers in the decision graph.

From Eqs. (3) to (4), it can be seen that $\rho(\boldsymbol{Y}_i)$ equals to the number of objects within $\boldsymbol{d}_c$ with respect to object $\boldsymbol{Y}_i$. $\delta(\boldsymbol{Y}_i)$ is measured by,

$$\delta(\boldsymbol{Y}_i) = \min_{i:\rho(\boldsymbol{Y}_j)>\rho(\boldsymbol{Y}_i)} \boldsymbol{dist}(\boldsymbol{Y}_i, \boldsymbol{Y}_j) \tag{5}$$

For the object with highest density, $\delta(\boldsymbol{Y}_i)$ is conventionally set to,

$$\delta(\boldsymbol{Y}_i) = \max_i \boldsymbol{dist}(\boldsymbol{Y}_i, \boldsymbol{Y}_j) \tag{6}$$

Note that if $\boldsymbol{Y}_i$ is local or global maxima in the density, $\delta(\boldsymbol{Y}_i)$ will be much larger than its typical nearest neighbor. Thus, objects with larger ρ and δ are considered as cluster centers, whereas objects with smaller ρ and larger δ are considered as outliers. Other objects are assigned to the same cluster as their nearest neighbor of higher density (see Fig. 7).

(d) *Input Parameter Optimization*: In each clustering method, there are several user-specified input parameters, which can significantly affect the shape of the cluster and the number of the cluster (Fig. 8). For hierarchical method, the cutting height of the dendrogram needs to be specified and the number of clusters varies with different cutting heights. For OPTICS, $\boldsymbol{\varepsilon}$ can simply be set to the maximum possible value, and Ankerst et al. (1999) showed that for $\boldsymbol{MinPts}$ using values between 10 and 20 would always lead to good results. However, the threshold for the reachability plot, which is used to extract clusters, still needs to be properly determined. For DPC, $\boldsymbol{d}_c$ can be chosen based on the rule that the average number of neighbors is around 1–2% of the total number of objects in the data set (Rodriguez and Laio, 2014). A threshold for ρ and δ needs to be defined to distinguish cluster centers, borders, and outliers. In this study, the average silhouette index (Rousseeuw, 1987) was employed to determine the optimal values of these parameters. Assume the data have been clustered via any clustering algorithm, such as OPTICS, into K clusters. For each object $\boldsymbol{Y}_i$, let $\boldsymbol{a}(\boldsymbol{Y}_i)$ represent the average distance of $\boldsymbol{Y}_i$ with all other object in the same cluster, and $\boldsymbol{b}(\boldsymbol{Y}_i)$ represent the smallest average distance of $\boldsymbol{Y}_i$ to any other cluster, of

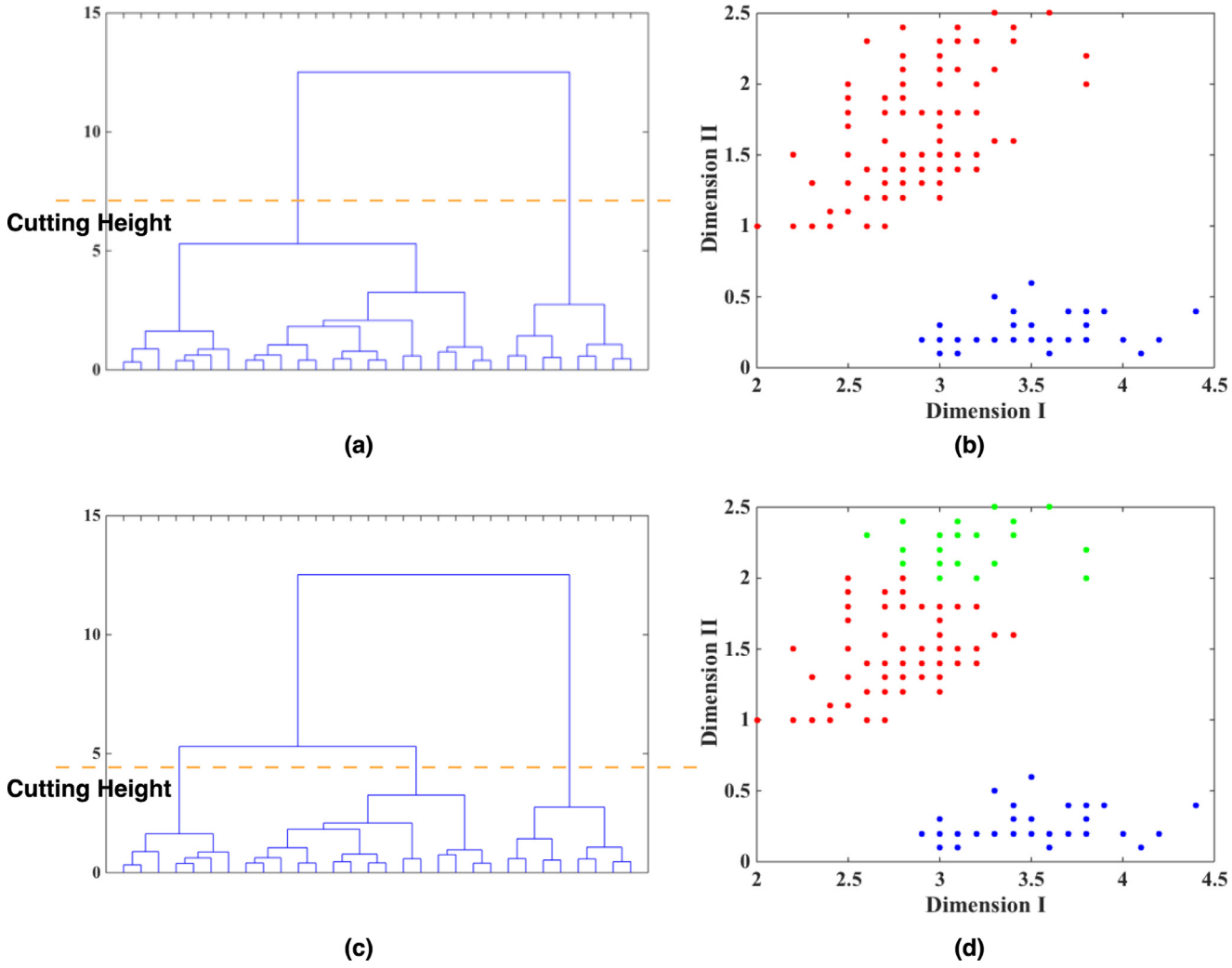

Fig. 8. Illustration of dependency of clustering results on input parameters. Take hierarchical clustering as an example. With a relatively high cutting height (a), two clusters (red and blue) were identified (b). As cutting height was reduced (c), one big cluster (red) was separated into two smaller clusters (d).

which $\boldsymbol{Y}_i$ does not belong to. Then the silhouette index of $\boldsymbol{Y}_i$ is defined as:

$$s(\boldsymbol{X}_i) = \frac{\boldsymbol{b}(\boldsymbol{Y}_i) - \boldsymbol{a}(\boldsymbol{Y}_i)}{\max\{\boldsymbol{a}(\boldsymbol{Y}_i),\ \boldsymbol{b}(\boldsymbol{Y}_i)\}} \tag{7}$$

From Eq. (7), it can be seen that $s(\boldsymbol{Y}_i)$ is bounded between −1 and 1. If $\boldsymbol{Y}_i$ has been assigned to a "correct" cluster, $s(\boldsymbol{Y}_i)$ will be close to 1. Contrarily, if $\boldsymbol{Y}_i$ has been assigned to a "wrong" cluster, $s(\boldsymbol{Y}_i)$ will be close to −1. $s(\boldsymbol{Y}_i)$ will be close to 0, if $\boldsymbol{Y}_i$ is located on the border of two natural clusters. By computing the average $s(\boldsymbol{Y}_i)$ over all objects in the entire dataset, the accuracy of the clustering results can be quantified.

With the average silhouette index as the optimization criterion, a "grid search" (Bergstra and Bengio, 2012) method was applied on determining the optimal value of each parameter. The optimal number of clusters can be determined simultaneously. For example, in OPTICS, we started with a relatively high threshold for the reachability-plot. In each iteration, the threshold was reduced by a small amount and the average $s(\boldsymbol{Y}_i)$ was computed and recorded based on the current partition. The iteration continues until the threshold was smaller than a specified baseline, e.g., the average reachability-distance of the reachability-plot. The optimal threshold was then determined as the one with the largest average $s(\boldsymbol{Y}_i)$. The same iterative procedure was applied to hierarchical clustering to determine optimal cutting height of dendrogram, and to DPC to determine the optimal threshold of ρ and δ.

2.5. Feature selection and cluster identification

The clustering accuracy is often lower in high dimensional feature space, which may be because most of features in the dataset may be irrelevant, redundant, or sometimes may even misguide results. Moreover, a large number of features make the clustering results difficult to interpret. Therefore, a feature selection method is required to improve the clustering accuracy. For supervised learning, feature selection can be trivial, i.e., only the features that are related to the given cluster labels are maintained. Nevertheless, for unsupervised learning, the cluster labels are unknown. Thus, finding the relevant subset of features and clustering the subset of the data must be accomplished simultaneously.

Assuming d to be the initial number of features, an exhaustive search of 2^d possible subsets need to be examined, which is computationally expensive. Therefore, in this study an alternative GA based method was applied to determine the optimal subset of features, as well as the optimal clustering results. The average silhouette index was used as the optimization criteria.

As one of the most popular search heuristic methods, GA has been widely used in generating solutions to optimization and searching problems (Yang and Honavar, 1997; Shahamat and Pouyan, 2015). Different from single-state methods (only one solution is evaluated at a time), e.g., simulated annealing, hill climbing, etc., GA is a "population" method that maintains a set of solutions evolving toward an optimal solution. The evolution usually starts from a population of randomly generated

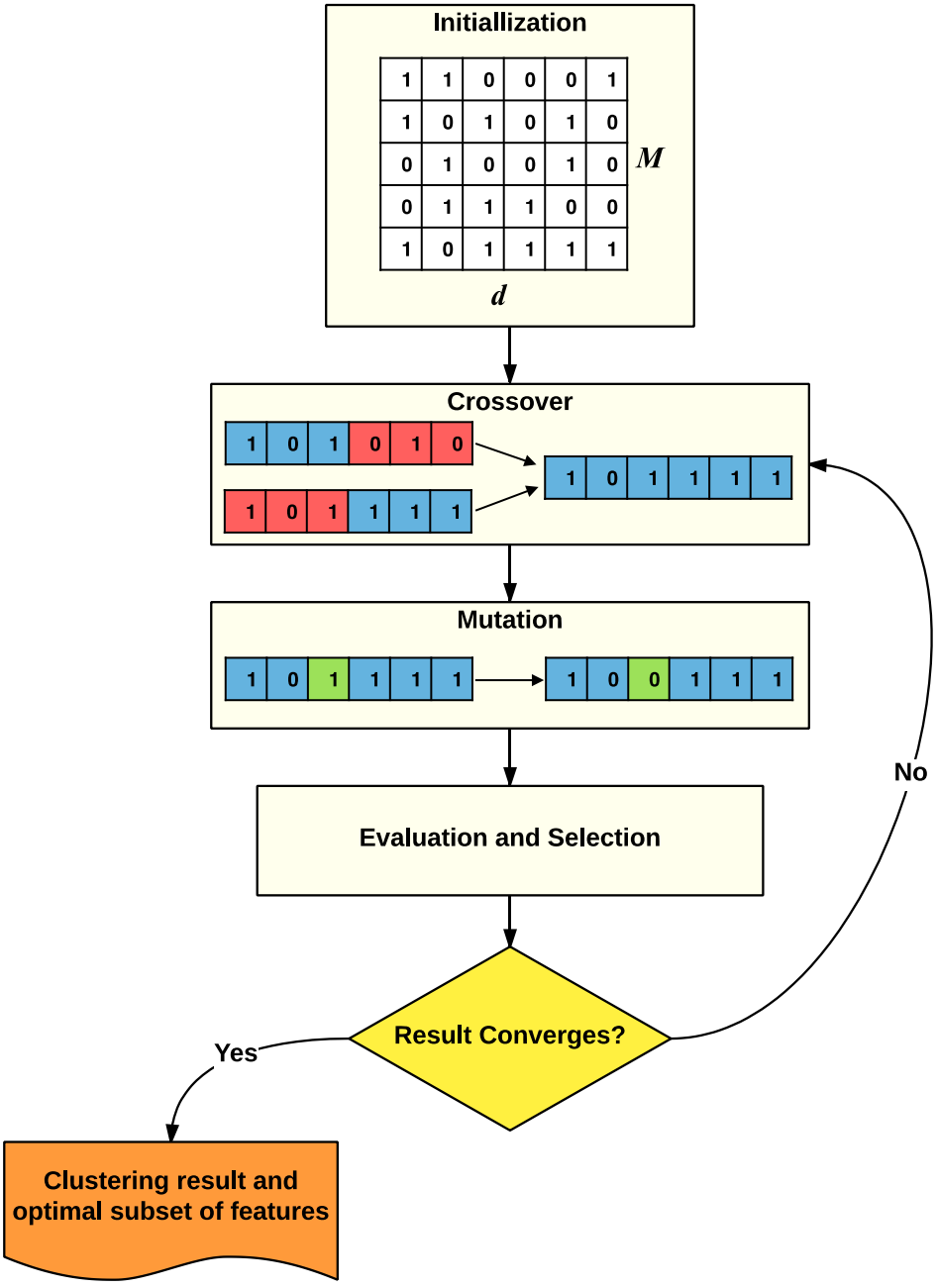

Fig. 9. Flowchart of GA for feature selection. In the $\boldsymbol{M}$-by-$\boldsymbol{d}$ matrix, each row represents a candidate solution, describing a subset of selected features. Each of the $\boldsymbol{d}$ bits in a row represents whether a feature is selected (1) or discarded (0).

solutions. In each iteration (or so called "generation"), "survivor solutions" with larger values of optimization criteria, i.e., the average silhouette index, are selected to form a new generation of solutions. These survival solutions can be generated from the crossover, which produced new solutions by randomly combining two current solutions, mutations, which randomly changes new solutions with a small probability, or from the initial population. The new generation of solutions is then used in the next iteration of the algorithm. Conventionally, the algorithm terminates when the best solution cannot be improved any further.

In this study, an array of $\boldsymbol{d}$ bits was used to represent the selected subset of features and the population size is represented using $\boldsymbol{M}$. Each bit in the array indicates the activation status of one specific feature: 1 indicates selected and 0 indicated discarded. The complete procedure of GA is described below (Fig. 9):

(1) Initialization: 400 candidate solutions were generated by randomly setting 1 or 0 for each bit in vectors.
(2) Crossover: two candidate solutions A and B were randomly selected from the current population. A value v between 1 and $\boldsymbol{d}$ was randomly selected. Then a new solution was formed by combining the feature bits 1 to v from A and feature bits $v + 1$ to $\boldsymbol{d}$ from B.
(3) Mutation: for each new generated solution, a mutation was applied by reversing bits in the vector with a probability of 0.1.
(4) Evaluation: the clustering method was applied on each candidate solution (i.e., a subset of selected features), and the average silhouette index was computed for each obtained partition.
(5) Selection: 280 solutions resulting in high average silhouette index were selected along with 120 solutions randomly selected from the rest of the solution (to increase the diversity of the population).
(6) If the result did converge, i.e., the average silhouette index of the best solution in the population keep increases, we iterated back to step 2. Otherwise, the clustering result with the largest average silhouette index and the corresponding selected subset of features were saved as the output.

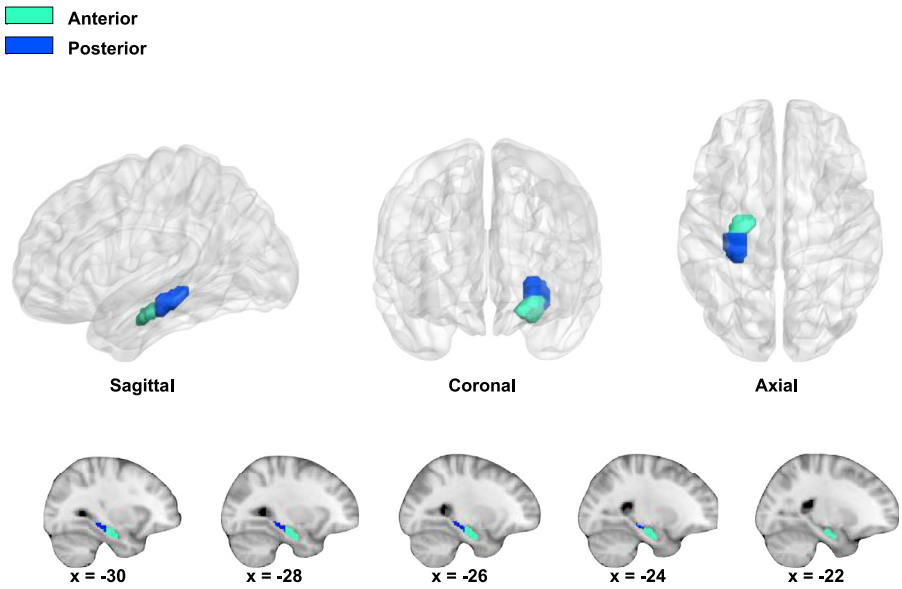

Fig. 10. Anatomical anterior-posterior segmentation used in this study. (Coordinates are in MNI space).

2.6. Volume level clustering

In order to determine whether characterizing layer-specific microcircuits using ultra-high field fMRI provides any advantages over conventionally computed voxel-level connectivity, the same clustering procedure enumerated above was also performed on the FC computed between hippocampal and DAN/DMN voxels during encoding/retrieval tasks. Specifically, let $\boldsymbol{Y} = \{\boldsymbol{Y}_1, \cdots, \boldsymbol{Y}_i, \cdots, \boldsymbol{Y}_N\}$ represent a set of $\boldsymbol{N}$ objects, i.e., number of hippocampal voxels. $\boldsymbol{Y}_i = (Y_{i1}, Y_{i2}, \cdots, Y_{id}) \in \mathbb{R}^d$, where $\boldsymbol{d}$ equals to the number of FC features computed between hippocampal voxels and voxels in the DAN/DMN, respectively. Subsequently, the same clustering and feature selection process was repeated on encoding and retrieval tasks, DAN and DMN ROIs, separately.

2.7. Comparison with anatomical anterior-posterior segmentation

In this study, clusters were identified based on the DAN/DMN-hippocampal FC during encoding/retrieval tasks, respectively. This provided a functional parcellation of the hippocampus, which was compared with anatomically delineated anterior and posterior hippocampal segments.

The hippocampus can be anatomically separated into head, body, and tails, with the head and body being considered as anterior, and the tail being considered as the posterior part. Various methods, such as landmark-based segmentation (Poppenk et al., 2013), percentile-based axis segmentation (Hackert et al., 2002; Greicius et al., 2003), a Talairach/MNI coordinate-based segmentation (Poppenk et al., 2013), have been used to define the anterior and posterior regions of the hippocampus. We employed the Talairach/MNI coordinate-based segmentation (Poppenk et al., 2013) which chose $y = -21$ in MNI space ($y = -20$ in Talairach space) as the border between anterior and posterior segmentations as shown in Fig. 10. This coordinate corresponds to the uncal apex, which is considered as the end of the posterior portion of the hippocampus (Destrieux et al., 2013).

Let $\boldsymbol{A} = \{\boldsymbol{A}_1, \boldsymbol{A}_2, \cdots, \boldsymbol{A}_M\}$ represent m anatomical parcels, and $\boldsymbol{F} = \{\boldsymbol{F}_1, \boldsymbol{F}_2, \cdots, \boldsymbol{F}_M\}$ denote n functional parcels identified by applying clustering methods on FC features. The similarity between these two parcellations was then quantified using Torres' method (Torres et al., 2008). The similarity matrix for A and F is an $\boldsymbol{m} \times \boldsymbol{n}$ matrix defined as:

$$\boldsymbol{S}_{\boldsymbol{A},\boldsymbol{F}} = \begin{bmatrix} \boldsymbol{S}_{11} & \cdots & \boldsymbol{S}_{1j} & \cdots & \boldsymbol{S}_{1n} \\ & & \vdots & & \\ \boldsymbol{S}_{i1} & \cdots & \boldsymbol{S}_{ij} & \cdots & \boldsymbol{S}_{in} \\ & & \vdots & & \\ \boldsymbol{S}_{m1} & \cdots & \boldsymbol{S}_{mj} & \cdots & \boldsymbol{S}_{mn} \end{bmatrix} \tag{8}$$

where $\boldsymbol{S}_{ij} = \boldsymbol{i}/\boldsymbol{u}$, which is Jaccard's Similarity Coefficient with $\boldsymbol{i}$ being the size of intersection and $\boldsymbol{u}$ being the size of the union of cluster sets $\boldsymbol{A}_i$ and $\boldsymbol{F}_j$. The similarity of parcellations $\boldsymbol{A}$ and $\boldsymbol{F}$ is then defined as:

$$\boldsymbol{Sim}(\boldsymbol{A}, \boldsymbol{F}) = \frac{\sum_{i \le m,\ j \le n} \boldsymbol{S}_{ij}}{\boldsymbol{max}(\boldsymbol{m}, \boldsymbol{n})} \tag{9}$$

From Eqs. (8) to (9), it can be seen that $0 \le \boldsymbol{Sim}(\boldsymbol{A}, \boldsymbol{F}) \le 1$, and $\boldsymbol{Sim}(\boldsymbol{A}, \boldsymbol{F}) = 1$ when two parcellations are identical.

The entire analysis pipeline proposed for investigating functional differentiation of the hippocampus and layer-specific microcircuitry between the hippocampus and the DAN and DMN during encoding/retrieval tasks are illustrated in Fig. 2.

3. Results

The optimal values of each input parameter determined for the three clustering methods are presented Tables 1 and 2 for layer-level and volume-level clustering, respectively. Using each clustering method, the hippocampal voxels were clustered into two different functional parcels based on their FC with (1) layer V of the DAN/DMN during the encoding task, and (2) layer II of the DAN/DMN during the retrieval task. This was true across methods. The obtained clusters were then mapped back to the image space and the resulting hippocampal parcels were overlaid on the anatomical image for the visualization.

Similar hippocampal parcellations were discovered using their FC with layer V of the DAN/DMN during the encoding task and layer II of the DAN/DMN during the retrieval task, and the average cluster similarity between DPC and hierarchical clustering, between DPC and OPTICS, and between hierarchical clustering and OPTICS, were 0.93, 0.95, and 0.92, respectively. For illustration, the clustering results obtained using the DPC method are shown in Fig. 11. The clustering results obtained using hierarchical clustering and OPTICS are shown in Supplementary Information Figs. S.1 and S.2. From Fig. 11, it can be seen that the hippocampus showed an anterior-posterior gradient along the long-axis,

Table 1
Estimated optimal values of each input parameter in layer-specific clustering. h: cutting height, and s: reachability threshold.

Method Name	Parameter	Left Hippocampus			
		DAN		DMN	
		Encoding Layer V	Retrieval Layer II	Encoding Layer V	Retrieval Layer II
DPC	ρ	9.03	7.13	8.29	8.50
	δ	3.15	2.82	3.14	3.04
Hierarchical	h	1.16	1.15	1.15	1.15
OPTICS	s	0.55	0.50	0.53	0.25

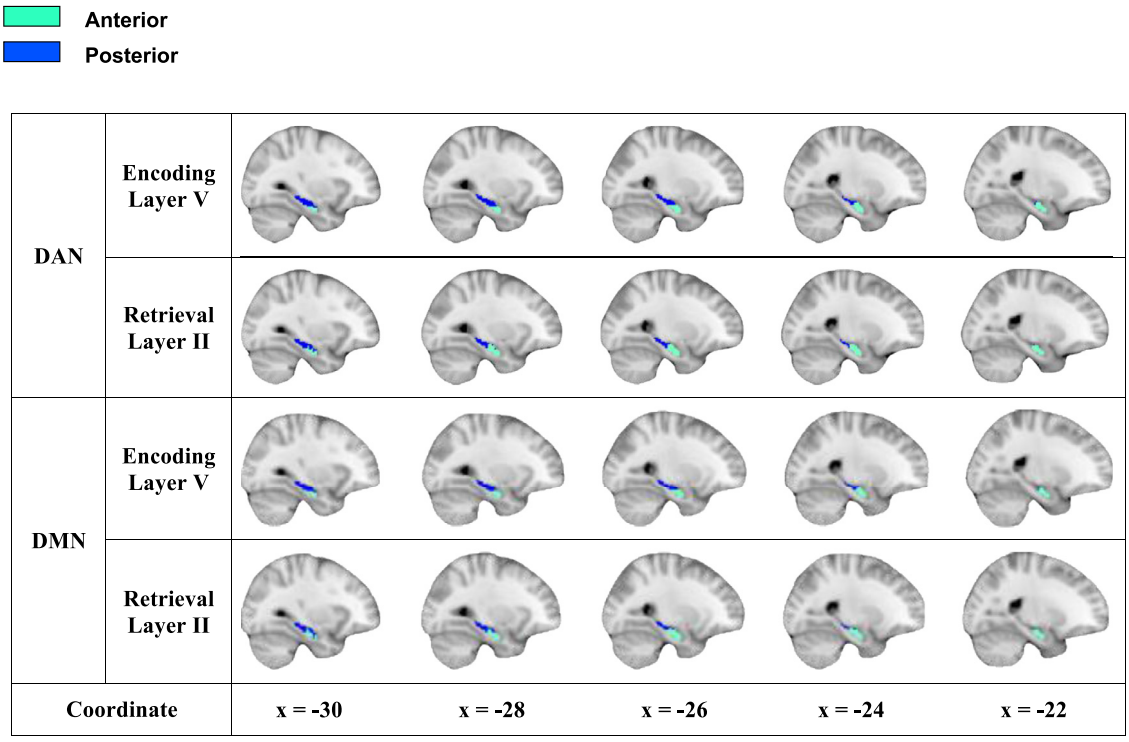

Fig. 11. Clusters of hippocampal voxels determined (using the DPC method) based on their functional connectivity with (1) layer V of the DMN/DAN during the encoding task, and (2) layer II of the DMN/DAN during the retrieval task. (Coordinates are in MNI space).

Table 2
Estimated optimal values of each input parameter in volume-level clustering. h: cutting height, and s: reachability threshold.

Method Name	Parameter	Left Hippocampus			
		DAN		DMN	
		Encoding	Retrieval	Encoding	Retrieval
DPC	ρ	7.59	6.38	5.61	7.93
	δ	0.09	0.13	0.18	0.12
Hierarchical	h	1.15	1.15	1.16	1.15
OPTICS	s	0.39	0.06	0.002	0.03

which is consistent with the anatomical anterior-posterior segmentation (Fig. 10).

To quantitatively characterize the identified clusters, the cluster similarity between our functionally obtained hippocampal parcels and anatomically defined anterior-posterior parcels (Fig. 10) was computed. The mean correlation between hippocampal voxels and selected vertices (using GA-based feature selection method) in layer V of the DAN/DMN (during the encoding task) and the layer II of the DAN/DMN (during the retrieval task) was also computed within anterior and posterior hippocampal regions (Table 3).

For the left hippocampus, during the encoding task, the average cluster similarity, over different clustering methods, between functional and anatomical parcellations for layer V of the DAN and DMN was 0.70 and 0.70, respectively. The absolute correlation observed between layer V of the DAN and the hippocampus was significantly larger than that between layer V of the DMN and the hippocampus as the p-values shown in Table 4, which is in line with our second hypothesis. A one-tailed 2-sample t-test was conducted to test whether the correlation of layer V of the DAN with the anterior hippocampal regions was significantly larger than that with the posterior hippocampal regions. The p-values obtained for different clustering methods were all close to 1, which did not provide evidence to support our third hypothesis for DAN part.

During the retrieval task, the average cluster similarity between functional and anatomical parcellations for layer II of the DAN and DMN was 0.70 and 0.77, respectively. The absolute correlation obtained between layer II of the DMN and the hippocampus was significantly larger than that between layer II of the DAN and the hippocampus as the p-values shown in Table 5, which was consistent with our second hypothesis. In addition, the correlation between layer II of the DMN and the posterior hippocampal regions was significantly larger than that with the anterior hippocampal regions (one-tailed 2-sample t-test; $p < 0.001$ for different clustering methods), considering the sign of the correlation. This result was in line with our third hypothesis for DMN part.

Table 3
Cluster similarity between functional and anatomical anterior-posterior parcellations using different clustering methods and mean correlation obtained within each cluster on the left side of the hippocampus.

Clustering Method	Feature Type	Task Name	DAN			DMN		
			Correlation		Sim.	Correlation		Sim.
			Anterior	Posterior		Anterior	Posterior	
DPC	Layer-specific	Encoding Layer V)	−0.36	0.36	0.70	−0.13	0.16	0.70
		Retrieval (Layer II)	0.09	−0.06	0.73	−0.39	0.31	0.77
	Volume-level	Encoding	0.20	0.04	0.69	0.02	0.12	0.69
		Retrieval	0.30	0.33	0.74	−0.01	−0.02	0.74
Hier.	Layer-specific	Encoding Layer V)	−0.36	0.35	0.70	−0.13	0.16	0.70
		Retrieval (Layer II)	−0.14	0.11	0.63	−0.41	0.34	0.77
	Volume-level	Encoding	0.48	−0.17	0.68	0.51	−0.18	0.69
		Retrieval	0.08	−0.05	0.72	0.01	0.02	0.74
OPTICS	Layer-specific	Encoding Layer V)	−0.35	0.34	0.70	−0.09	0.10	0.70
		Retrieval (Layer II)	−0.14	0.07	0.73	−0.36	0.27	0.77
	Volume-level	Encoding	0.51	−0.18	0.69	0.02	0.03	0.71
		Retrieval	−0.33	0.41	0.57	0.21	−0.09	0.74

Table 4
Comparison of the absolute correlations obtained between the DAN with the hippocampus and the DMN with the hippocampus during the encoding task by conducting one-tailed two-sample *t*-test (H_0: correlation of DAN and the hippocampus ≤ correlation of the DMN and the hippocampus).

Feature Type	Clustering Method	Left Hippocampus					
		Mean Absolute Correlation				P-value	
		DAN		DMN			
		Anterior	Posterior	Anterior	Posterior	Anterior	Posterior
Layer-specific (Layer V)	DPC	0.39	0.39	0.34	0.35	< 0.001	0.005
	Hierarchical	0.38	0.39	0.34	0.35	0.004	0.009
	OPTICS	0.37	0.38	0.34	0.35	0.002	0.007
Volume-level	DPC	0.51	0.18	0.51	0.18	0.500	0.500
	Hierarchical	0.48	0.17	0.51	0.18	0.750	0.564
	OPTICS	0.51	0.18	0.45	0.19	0.170	0.507

Table 5
Comparison of the absolute correlations obtained between the DMN with the hippocampus and the DAN with the hippocampus during the retrieval task by conducting one-tailed two-sample *t*-test (H_0: correlation of the DMN with the hippocampus ≤ correlation of the DAN and the hippocampus).

Feature Type	Clustering Method	Left Hippocampus					
		Mean Absolute Correlation				P-value	
		DAN		DMN			
		Anterior	Posterior	Anterior	Posterior	Anterior	Posterior
Layer-specific (Layer II)	DPC	0.37	0.37	0.51	0.41	< 0.001	0.002
	Hierarchical	0.34	0.38	0.51	0.41	< 0.001	0.023
	OPTICS	0.45	0.28	0.50	0.40	0.015	< 0.001
Volume-level	DPC	0.32	0.30	0.35	0.24	0.298	0.932
	Hierarchical	0.23	0.27	0.31	0.28	0.053	0.444
	OPTICS	0.33	0.41	0.32	0.26	0.540	0.973

For volume level analysis, i.e. clustering of hippocampal voxels based on their FC with voxels in DAN/DMN volume (as opposed to layer II and layer V of the DAN/DMN as before), similar parcellations were discovered using different clustering methods, and the average cluster similarity between DPC and hierarchical clustering, between DPC and OPTICS, and between hierarchical clustering and OPTICS, were 0.96, 0.88, and 0.87, respectively. For illustration, the clustering results using DPC are shown in Fig. 12, and the clustering results using hierarchical clustering and OPTICS are shown in supplementary information (Figs. S.3 and S.4).

As shown in Fig. 12, an anterior-posterior gradient was obtained as well. The cluster similarity between functional and anatomical parcellations, and the mean correlation within anterior and posterior regions were also computed for volume level clustering. As shown in Table 3, the average cluster similarity for the DAN (during the encoding task) and the DMN (during the retrieval task) were 0.69 and 0.74, respectively, which were qualitatively less than the value obtained using the layer-specific data. During the encoding task, the correlation between DAN and the hippocampus was not significantly greater than the correlation between DMN and the hippocampus ($p > 0.05$) for all three clustering methods (Table 4), whereas during the retrieval task, the correlation between DMN and the hippocampus was not significantly greater than the correlation between DAN and the hippocampus for all three methods (Table 5). This result was different from the result obtained using layer-specific data. It was also contradictory to our second hypothesis. The correlations between anterior and posterior hippocampal regions with DAN/DMN for encoding/retrieval tasks were also compared using one-tailed 2-sample *t*-test. During the encoding task, the p-values obtained for DPC, hierarchical, and OTPICS were 0.019, < 0.001, and 0.02, respectively, whereas during the retrieval task, the p-values obtained for these three methods were 1, 1, and 0.436, respectively. This result provided evidence for our third hypothesis for only the

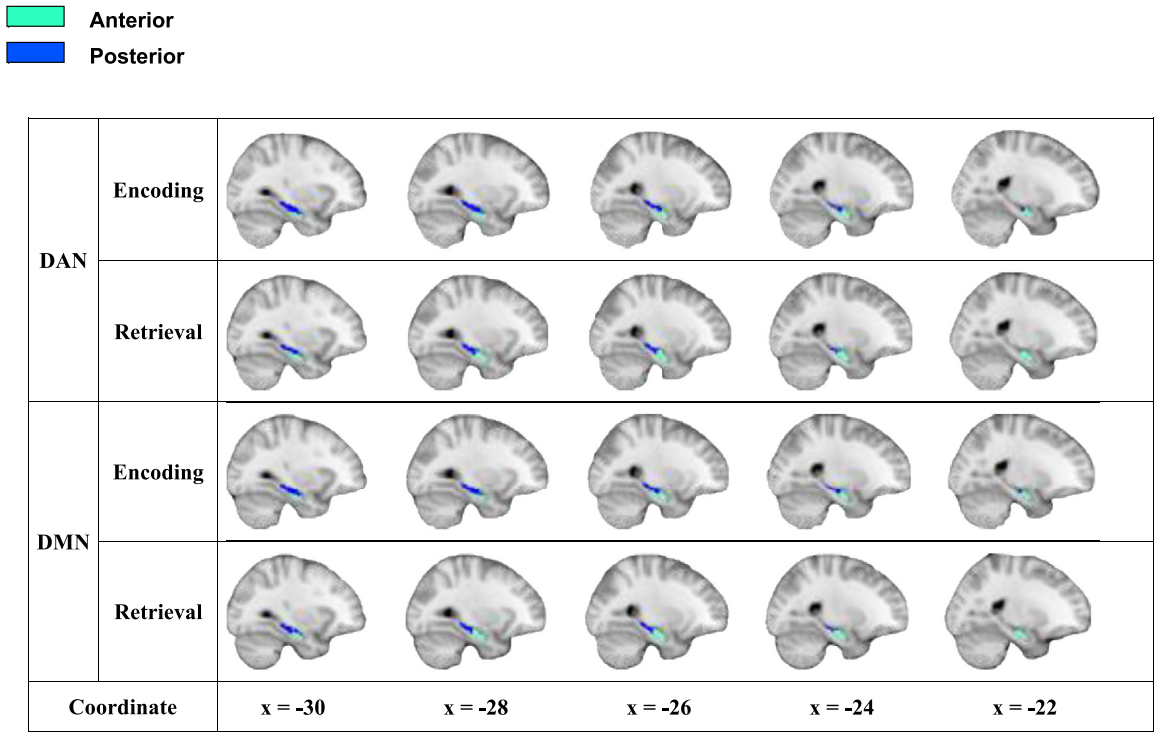

Fig. 12. Clusters of hippocampal voxels determined (using the DPC method) based on their functional connectivity DMN/DAN volume during encoding and retrieval tasks. (Coordinates are in MNI space).

DAN part considering the sign of the correlation, not for the DMN part.

4. Discussion

In this work, we investigated functional differentiation of the hippocampus and the connectivity between the hippocampus and DAN/DMN regions during encoding/retrieval tasks. Given the predictions obtained from the HIPER/HERNET model and known anatomical pathways between these networks and the hippocampus, we tested four hypotheses as described in the Introduction section. In order to do so, we investigated the connectivity between the hippocampus and layer V of the DAN during the encoding task, and between the hippocampus and layer II of the DMN during the retrieval task. The proposed first, second and fourth hypotheses were confirmed, whereas the third hypothesis was partially confirmed for DMN part (considering sign of the correlation), not for DAN part. The discussion of results is organized as follows. First, we discuss the results obtained by the validation of the anterior-posterior differentiation of the hippocampus using the FC between (1) hippocampal voxels and layer V of the DAN during the encoding task, and (2) hippocampal voxels and layer II of the DMN during the retrieval task. Second, we discuss the connectivity between the hippocampus and the DAN/DMN during encoding/retrieval tasks. Third, we discuss the layer-specific functional microcircuits between the layer V of the DAN and the hippocampus during the encoding task, and between the layer II of the DMN and the hippocampus during the retrieval task. Fourth, we discuss the importance of ultra-high field functional neuroimaging in developing accurate and robust models of functional connectivity. Finally, we discuss the functional differentiation of the hippocampus along the long-axis.

4.1. Anterior-Posterior functional differentiation of the hippocampus

The idea that the anterior and posterior parts of the hippocampus may serve different functions emerged half a century ago (Nadel, 1968). More recently, Robinson et al. (2015) conducted meta-analyses and found an anterior-posterior long-axis segmentation on both the left and right hippocampi. Duarte et al. (2014) studied functional specialization of the hippocampus using fMRI and a virtual reality 3D paradigm. They found a functional dichotomy whereby the anterior/posterior hippocampus shows antagonistic processing patterns for spatial encoding and retrieval of 3D spatial information. Prince et al. (2005) also provided evidence for an anterior-posterior parcellation that corresponded to encoding/retrieval processes. Not just in the hippocampus, but Wang et al. (2016) showed this to be true in other regions of the medial temporal lobe, such as the perirhinal cortex (PRC) as well. Specifically, they showed preferential functional connection of the anterior PRC with the DAN and the posterior PRC with the DMN.

In this study, the functional specialization of the hippocampus has been investigated by using unsupervised clustering of functional connectivity between the hippocampus and layer II/V of the DAN/DMN during encoding/retrieval processes, respectively. Our results yielded a consistent anterior-posterior long-axis parcellation, which showed high cluster similarity across clustering methods based on completely different principles. This result indicates that during the encoding/retrieval processes, there is a robust anterior-posterior functional differentiation along the long-axis of the hippocampus.

4.2. Layer-specific connectivity between the DAN/DMN and hippocampus

The anatomical pathways between the hippocampus and DAN/DMN have been studied using invasive animal models by many researchers (Sugar et al., 2011; Thomson and Bannister, 2003; Thomson and Lamy, 2007). During an encoding task, deeper infra-granular layers (specifically, layer V) of the DAN project to the hippocampus, whereas the hippocampal output reaches primarily more superficial supra-granular layers (specifically, layer II) of the DMN. This layer-specific organization has also been reported by many anatomical studies. However, it has never been directly investigated using connectivity based non-invasive methods in humans.

This layer-specific pathway between the hippocampus and DAN/DMN is not exclusive since pathways which originate/terminate in other layers of the cortex may also contribute to the hippocampal input or output. This is not surprising given the highly complex underlying microcircuitry and given that signals between any two brain regions can relay via multiple structures including the thalamus. However, the pathways between the hippocampus and layers II and V of the DMN/DAN seem to be the dominant ones based on prior invasive animal literature (Shepard and Grillner, 2010; Thomson and Lamy, 2007) and therefore we have chosen to test them in this study.

We investigated the connectivity between the hippocampus and the DAN/DMN using FC between layer V of the DAN/DMN and the hippocampus during the encoding task, and between layer II of the DAN/DMN and the hippocampus during the retrieval task. During the encoding task, the correlation observed between layer V of the DAN and the hippocampus was significantly larger than that between layer V of the DMN and the hippocampus. Contrarily, during the retrieval task, the correlation obtained between layer II of the DMN and the hippocampus was significantly larger than that between layer II of the DAN and the hippocampus. Together, these findings provide evidence that the output from layer V of the DAN likely drives the hippocampus during encoding, whereas during retrieval, the output from the hippocampus is likely relayed as inputs to layer II of the DMN. Given that Pearson's correlation is a directionless quantity, our inference of directionality is indirect at best, based on known directionality of the underlying anatomical projections.

4.3. Layer-specific functional pathway between the DAN/DMN and hippocampus

Considering the directionality of signal projection during encoding/retrieval processes and the HERNET model, the information flow between different layers of the DAN/DMN and different regions of the hippocampus should follow the pattern: layer V of the DAN → anterior hippocampus → posterior hippocampus → layer II of the DMN. Thus, we hypothesized that during an encoding task, layer V of the DAN mush show stronger correlation with anterior hippocampal regions than with posterior hippocampal regions, whereas during retrieval task, layer II of the DMN must exhibit stronger correlation with posterior hippocampal regions than with anterior hippocampal regions. Our results provide partial support for this hypothesis, i.e., only the DMN part was confirmed during retrieval task considering the sign of the correlation (negative in anterior, positive in posterior), but not for DAN part during encoding task. However, if we only consider the magnitude of the correlation ignoring its sign, the third hypothesis was not true for both the DAN and DMN part.

4.4. High-resolution functional imaging: layer vs volume data

Recent advances in ultra-high field fMRI have provided a non-invasive way of investigating cortical columns. This technique provides several advantages over conventional field strengths, e.g., improved spatial resolution, increased signal to noise ratio, etc. More importantly, this technique makes it feasible to examine layer-specific brain activation across different brain areas. Several recent studies have showed that investigating changes in fMRI activation as a function of laminar depth can lead to more precise results (Olman et al., 2012; Kok et al., 2016). In this study, we investigated functional differentiation of the hippocampus along the long-axis using unsupervised clustering of layer-specific functional connectivity between the hippocampus and the DAN/DMN regions. The same clustering process was also applied on the functional connectivity between the hippocampus and the DAN/DMN volume. As we expected, the layer-specific data led to more definitive results, i.e., the proposed first, second and forth hypotheses were confirmed, whereas the third hypothesis was partially confirmed for DMN part (considering sign of the correlation), not for DAN part. However, using volume-level data, only the first hypothesis was confirmed and the third hypothesis (only for DAN part with sign of the correlation being considered) was partially confirmed. Therefore, it is important to note the relevance of high-resolution functional neuroimaging as the field progresses toward developing more accurate and robust network models of brain function in general and hippocampal function in specific.

4.5. Long-axis differentiation of the hippocampus

Recent evidence has suggested that there is an anterior-posterior functional differentiation of the hippocampus along the long-axis. In Lepage's HIPER model (Lepage et al., 1998) and more recently Kim's HERNET mode (Kim, 2015), the anterior and posterior hippocampus are posited to be more associated with encoding and retrieval processes, respectively. This encoding/retrieval dichotomy faced conflicting evidence from some meta-analyses and studies. Schacter and Wagner (1999) reviewed data from diverse fMRI studies and observed that both the anterior and posterior hippocampal regions were associated with the encoding activation. Kumaran and Maguire (2006), Poppenk et al. (2008), and Zweynert et al. (2011) found that most encoding studies used novel stimuli, which were associated with the anterior hippocampus. On the other hand, Poppenk et al., 2010a2010b) observed that familiar stimuli were associated with the posterior hippocampus and superior source memory. Together, these studies suggest that the encoding/retrieval differentiation cannot rely on findings that link the anterior/posterior hippocampus to novel/familiar stimuli.

Although the encoding/retrieval dichotomy is predominant in humans, many alternative specializations have also been proposed. A motivational processing model has been proposed with the anterior hippocampus being mainly engaged in "hot" processing (emotion/motivation), whereas the posterior hippocampus being mainly associated with "cold" processing (cognition) (Murty et al., 2011). Robinson et al. (2015)(2016). also found support for this hypothesis based on hippocampal parcellations obtained from meta-analyses, resting state fMRI connectivity and diffusion tensor imaging (). However, Wolosin et al. (2012) found that the posterior hippocampus also contributed to negative emotional memory. Some other studies have proposed that the posterior hippocampus is especially important for spatial processing, whereas the anterior hippocampus may be important for episodic memory or other functions (Ryan et al., 2010; Hirshhorn et al., 2012). This model was undercut by evidence that the anterior hippocampus also plays a spatial role (Woollett and Maguire, 2012).

In this study, our results provided partial support for HIPER/HERNET model. The strength of evidence in favor of the HERNET model was superior with layer-specific data compared to conventional volume data. A consistent anterior to posterior long-axis segmentation was found during encoding/retrieval tasks. We also found that during an encoding task, the hippocampus was more correlated with the layer V of the DAN, whereas during a retrieval task, the hippocampus was more associated with layer II of the DMN. However, we did not find support for stronger correlation of layer V of the DAN and the anterior portions during the encoding task. Our results also did not support the prediction of stronger correlation of layer II of the DMN and the posterior hippocampal segments during the retrieval task (ignoring the sign of the correlation). Together, these results suggest that the underlying neurophysiology of the hippocampus and its interaction with the neocortex under various neurocognitive contexts is far more complex than relatively simplistic models currently available. Our study demonstrates that it will take better quality data in terms of spatial-temporal resolution in order to build better models of hippocampal function and specialization.

4.6. Limitations

The present study has a few limitations that may be addressed in future research. First, in this study, the cortical layers were delineated

using the equidistant model (Khan et al., 2011), i.e., the cortical layers were reconstructed at a relatively fixed distance to the cortical interface. An alternative way is to solve the Laplace equation within the interfaces of the cortex and generate cortical profiles along the gradient of the solution. This model is the so called "Laplace model", which was proposed by Jones et al. (2000). Recently, Waehnert et al. (2014) proposed a novel equivolume model, which was claimed to have better performance than both the equidistant model as well as the Laplace model. Future work should evaluate the performance of this equivolume model. If found to be superior, the results presented in this work need to be replicated with more accurate reconstructions of cortical layers.

Second, our results consistently showed an anterior-posterior gradient in the left hippocampus by using the functional connectivity between the hippocampus and layer II/V of DAN/DMN ROIs during encoding/retrieval processes, respectively. This pattern was consistent with encoding/retrieval dichotomy that was proposed by HIPER/HERNET model. However, this pattern faced conflicting evidence from other studies (Schacter and Wagner, 1999). In addition, many alternative specializations have also been proposed, explaining the anterior-posterior segmentation in different perspectives, e.g., motivational processing model (Murty et al., 2011), etc. Given the complexity of underlying neurophysiology of the hippocampus and its interaction with neocortex under various neurocognitive contexts, it might be beneficial to find a way to reconcile different hippocampal models.

Third, in this study, all hypotheses were validated only on the left hippocampus. Our task involved factual memories of objects, pictures of scenes, and words, which likely preferentially recruits the left hippocampus (Burgess et al., 2002; Glosser et al., 1995). However, it is necessary to replicate the same on the right hippocampus, using tasks that preferentially activate the right hippocampus, to obtain more comprehensive and complete results. This should be done in future work.

Fourth, we explore the hypotheses both by considering and ignoring the sign of the correlation. This creates two different scenarios under which the hypotheses are considered. While this is not ideal, it is necessitated because arguments in favor of both approaches exist in the literature. Those in favor of using the sign argue about the so called antagonistic relationship between DMN and DAN and its relevance for brain function in health and disease (Owens et al., 2020). However, this relevance is neither straight-forward nor universal as the proponents themselves acknowledge in (Owens et al., 2020): "These findings indicate a complicated relationship between DMN/DAN anticorrelation and demographics, neuropsychological function, and psychiatric problems". Those against using the sign argue that linear association between signals is important and we cannot over-emphasize the sign of the correlation between signals given that two signals may have a strong linear relationship and yet may exhibit negative correlation due to phase differences. Further, recent reports indicate a dissociation between glucose metabolism and blood oxygenation in the DMN (Stiernman et al., 2021), which makes it difficult to (over) interpret the sign. In fact, using simultaneous PET/fMRI, Stiernman et al. (2021) convincingly demonstrate that task-positive and -negative BOLD responses (especially in the DMN/DAN system) do not reflect antagonistic patterns of synaptic metabolism. Given this ambiguity in the literature, we have presented results both with and without the sign as we do not want to take sides in this debate. Once the debate is settled in the literature, the corresponding results in our manuscript automatically become more relevant.

5. Conclusion

As one of the most important components in the brain of different species, the hippocampus plays crucial role in episodic memory and spatial navigation. Recent neuroimaging evidence suggests that there may be an anterior-posterior functional specialization of the hippocampus along the long-axis. Moreover, Lepage's HIPER model and Kim's HERNET model indicated that the anterior and posterior hippocampal regions were associated with memory encoding and retrieval, respectively. This model received support from many meta-analyses studies, but it also faced conflicting evidence from the outset.

In this study, we investigated the functional differentiation of the hippocampus using their functional connectivity with layer II/V of the DAN/DMN ROIs during encoding and retrieval processes. Given HIPER/HERNET model and anatomical layer-specific connection between the hippocampus and the DAN/DMN, four hypotheses were also proposed. Our results revealed a consistent anterior-posterior pattern, which showed high cluster similarity with an anatomical anterior-posterior segmentation. Meanwhile, the results demonstrated that during an encoding task, the hippocampus was more correlated with the layer V of the DAN, whereas during a retrieval task, the hippocampus was more associated with layer II of the DMN. However, we did not find support for stronger correlation of layer V of the DAN and the anterior portions during the encoding task, neither with stronger correlation of layer II of the DMN and the posterior portions during the retrieval task (ignoring the sign of the correlation).

The same clustering process was also applied on volume-level data in comparison with layer-specific data. As we expected, the results provided by layer-specific data were more definitive, which suggested that it is necessary to use a better quality data, in terms of spatial-temporal resolution, to build more precise and robust models of hippocampal function.

Data and code availability statement

Data and code used in this work is available upon request.

Supplementary materials

Supplementary material associated with this article can be found, in the online version, at doi:10.1016/j.neuroimage.2022.119078.

Credit authorship contribution statement

Gopikrishna Deshpande: Conceptualization, Methodology, Investigation, Resources, Writing – original draft, Supervision, Project administration, Funding acquisition. **Xinyu Zhao:** Software, Validation, Formal analysis, Data curation, Writing – original draft, Visualization. **Jennifer Robinson:** Conceptualization, Methodology, Investigation, Resources, Writing – original draft, Supervision, Funding acquisition.

References

Das, S.R., Mechanic-Hamilton, D., Pluta, J., Korczykowski, M., Detre, J.A., Yushkevich, P.A., 2011. Heterogeneity of functional activation during memory encoding across hippocampal subfields in temporal lobe epilepsy. Neuroimage 58 (4), 1121–1130.

Yushkevich, P.A., Wang, H., Pluta, J., Das, S.R., Craige, C., Avants, B.B., Weiner, M.W., Mueller, S., 2010. Nearly automatic segmentation of hippocampal subfields in in vivo focal T2-weighted MRI. Neuroimage 53 (4), 1208–1224.

Heckemann, R.A., Keihaninejad, S., Aljabar, P., Gray, K.R., Nielsen, C., Rueckert, D., Hajnal, J.V., Hammers, A., 2011. Automatic morphometry in Alzheimer's disease and mild cognitive impairment. Neuroimage 56 (4), 2024–2037.

Lukiw, W.J., 2007. Micro-RNA speciation in fetal, adult and Alzheimer's disease hippocampus. Neuroreport 18 (3), 297–300.

Zhou, Y., Dougherty, J.H., Hubner, K.F., Bai, B., Cannon, R.L., Hutson, R.K., 2008. Abnormal connectivity in the posterior cingulate and hippocampus in early Alzheimer's disease and mild cognitive impairment. Alzheimers Dement. 4 (4), 265–270.

Scheff, S.W., Price, D.A., 2006. Alzheimer's disease-related alterations in synaptic density: neocortex and hippocampus. J. Alzheimers Dis. 9, 101–115.

Campbell, S., MacQueen, G., 2004. The role of the hippocampus in the pathophysiology of major depression. J. Psychiatry Neurosci. 29 (6), 417–426.

Stockmeier, C.A., Mahajan, G.J., Konick, L.C., Overholser, J.C., Jurjus, G.J., Meltzer, H.Y., Uylings, H.B.M., Friedman, L., Rajkowska, G., 2004. Cellular changes in the postmortem hippocampus in major depression. Biol. Psychiatry 56 (9), 640–650.

Rosso, I.M., Cintron, C.M., Steingard, R.J., Renshaw, P.F., Young, A.D., Yurgelun–Todd, D.A., 2005. Amygdala and hippocampus volumes in pediatric major depression. Biol. Psychiatry 57 (1), 21–26.

MacQueen, G., Frodl, T., 2011. The hippocampus in major depression: evidence for the convergence of the bench and bedside in psychiatric research? Mol. Psychiatry 16 (3), 252–264.

Astur, R.S., St Germain, S.A., Tolin, D., Ford, J., Russell, D., Stevens, M., 2006. Hippocampus function predicts severity of post-traumatic stress disorder. Cyberpsychol. Behav. 9 (2), 234–240.

Javidi, H., Yadollahie, M., 2012. Post-traumatic stress disorder. Int. J. Occup. Environ. Med. 3 (1), 2–9.

Harrison, P.J., 2004. The hippocampus in schizophrenia: a review of the neuropathological evidence and its pathophysiological implications. Psychopharmacology 174 (1), 151–162 *(Berl.)*.

Heckers, S., 2001. Neuroimaging studies of the hippocampus in schizophrenia. Hippocampus 11 (5), 520–528.

Grace, A.A., 2012. Dopamine system dysregulation by the hippocampus: implications for the pathophysiology and treatment of schizophrenia. Neuropharmacology 62 (3), 1342–1348.

Nadel, L., 1968. Dorsal and ventral hippocampal lesions and behavior. Physiol. Behav. 3, 891–900.

de Wael, R.V., Lariviere, S., Caldairou, B., Hong. D. S. Margulies, S.J., Jefferies, E., Bernasconi, A., Smallwood, J., Bernasconi, N., Bernhardt, B.C., 2018. Anatomical and microstructural determinants of hippocampal subfield functional connectome embedding. Proc. Natl. Acad. Sci. USA. 115 (40), 10154–10159.

Lepage, M., Habib, R., Tulving, E., 1998. Hippocampal PET activations of memory encoding and retrieval: the HIPER model. Hippocampus 8 (4), 313–322.

Spaniol, J., Davidson, P.S.R., Kim, A.S.N., Han, H., Moscovitch, M., Grady, C.L., 2009. Event-related fMRI studies of episodic encoding and retrieval: meta-analyses using activation likelihood estimation. Neuropsychologia 47 (8–9), 1765–1779.

Nadel, L., Hoscheidt, S., Ryan, L.R., 2013. Spatial cognition and the hippocampus: the anterior-posterior axis. J. Cogn. Neurosci. 25 (1), 22–28.

Baumann, O., Mattingley, J.B., 2013. Dissociable representations of environmental size and complexity in the human hippocampus. J. Neurosci. 33 (25), 10526–10533.

Kim, H., 2015. Encoding and retrieval along the long axis of the hippocampus and their relationships with dorsal attention and default mode networks: the HERNET model. Hippocampus 25 (4), 500–510.

Kim, H., 2010. Dissociating the roles of the default-mode, dorsal, and ventral networks in episodic memory retrieval. Neuroimage 50 (4), 1648–1657.

Chun, M.M., Golomb, J.D., Turk-Browne, N.B., 2011. A taxonomy of external and internal attention. Annu. Rev. Psychol. 62, 73–101.

Buckner, R.L., Andrews-Hanna, J.R., Schacter, D.L., 2008. The brain's default network. Ann. N. Y. Acad. Sci. 1124 (1), 1–38.

Corbetta, M., Shulman, G.L., 2002. Control of goal-directed and stimulus-driven attention in the brain. Nat. Rev. Neurosci. 3 (3), 201–215.

Schacter, D.L., Wagner, A.D., 1999. Medial temporal lobe activations in fMRI and PET studies of episodic encoding and retrieval. Hippocampus 9 (1), 7–24.

Kumaran, D., Maguire, E.A., 2006. An unexpected sequence of events: mismatch detection in the human hippocampus. PLoS Biol. 4 (12), 2372–2382.

Poppenk, J., Walia, G., McIntosh, A.R., Joanisse, M.F., Klein, D., Köhler, S., 2008. Why is the meaning of a sentence better remembered than its form? An fMRI study on the role of novelty-encoding processes. Hippocampus 18 (9), 909–918.

Zweynert, S., Pade, J.P., Wüstenberg, T., Sterzer, P., Walter, H., Seidenbecher, C.I., Richardson-Klavehn, A., Düzel, E., Schott, B.H., 2011. Motivational salience modulates hippocampal repetition suppression and functional connectivity in humans. Front. Hum. Neurosci. 5, 144 no. November.

Poppenk, J., Köhler, S., Moscovitch, M., 2010a. Revisiting the novelty effect: when familiarity, not novelty, enhances memory. J. Exp. Psychol. Mem. Cogn. 36 (5), 1321–1330.

Poppenk, J., McIntosh, A.R., Craik, F.I.M., Moscovitch, M., 2010b. Past experience modulates the neural mechanisms of episodic memory formation. J. Neurosci. 30 (13), 4707–4716.

Murty, V.P., Ritchey, M., Adcock, R.A., LaBar, K.S., 2011. Reprint of: fMRI studies of successful emotional memory encoding: a quantitative meta-analysis. Neuropsychologia 49 (4), 695–705.

Robinson, J.L., Barron, D.S., Kirby, L.A.J., Bottenhorn, K.L., Hill, A.C., Murphy, J.E., Katz, J.S., Salibi, N., Eickhoff, S.B., Fox, P.T., 2015. Neurofunctional topography of the human hippocampus. Hum. Brain Mapp. 36 (12), 5018–5037.

Robinson, J.L., Salibi, N., Deshpande, G., 2016. Functional connectivity of the left and right hippocampi: evidence for functional lateralization along the long-axis using meta-analytic approaches and ultra-high field functional neuroimaging. Neuroimage 135, 64–78.

Swanson, L.W., Cowan, W.M., 1977. An autoradiographic study of the organization of the efferent connections of the hippocampal formation in the rat. J. Comp. Neurol. 172 (1), 49–84.

Thomson, A.M., Bannister, A.P., 2003. Interlaminar connections in the neocortex. Cereb. Cortex 13 (1), 5–14.

Shepard, G.M., Grillner, S., 2010. Handbook of Brain Microcircuits, p. 46 *Handbook of Brain Microcircuits.*.

Thomson, A.M., Lamy, C., 2007. Functional maps of neocortical local circuitry. Front. Neurosci. 1 (1), 19–42.

Dasgupta, S., Long, P.M., 2005. Performance guarantees for hierarchical clustering. J. Comput. Syst. Sci. 70, 555–569.

Ankerst, M., Breunig, M.M., Kriegel, H.P., Sander, J., 1999. Optics: ordering points to identify the clustering structure. ACM Sigmod. Rec. 49–60.

Rodriguez, A., Laio, A., 2014. Machine learning. Clustering by fast search and find of density peaks. Science 344 (6191), 1492–1496.

Dy, J.G., Brodley, C.E., 2004. Feature selection for unsupervised learning. J. Mach. Learn. Res. 5, 845–889.

Bradley, P.S., Mangasarian, O.L., 1998. Feature selection via mathematical programming. INFORMS J. Comput. 10 (2), 209–217.

Poppenk, J., Evensmoen, H.R., Moscovitch, M., Nadel, L., 2013. Long-axis specialization of the human hippocampus. Trends Cogn. Sci. 17 (5), 230–240 *(Regul. Ed.)*.

Ashburner, J., 2012. SPM: a history. Neuroimage 62 (2), 791–800.

Behzadi, Y., Restom, K., Liau, J., Liu, T.T., 2007. A component based noise correction method (CompCor) for BOLD and perfusion based fMRI. Neuroimage 37 (1), 90–101.

Burgess, N., Maguire, E.A., O'Keefe, J., 2002. The human hippocampus and spatial and episodic memory. Neuron 35 (4), 625–641.

Fischl, B., 2012. FreeSurfer. Neuroimage 62 (2), 774–781.

Dale, A.M., Fischl, B., Sereno, M.I., 1999. Cortical Surface-based analysis: I. Segmentation and surface reconstruction. Neuroimage 9 (2), 179–194.

Fischl, B., Sereno, M.I., Dale, A.M., 1999. Cortical surface-based analysis: II: inflation, flattening, and a surface-based coordinate system. Neuroimage 9 (2), 195–207.

Fischl, B., Dale, A.M., 2000. Measuring the thickness of the human cerebral cortex from magnetic resonance images. Proc. Natl. Acad. Sci. USA. 97 (20), 11050–11055.

Han, X., Jovicich, J., Salat, D., van der Kouwe, A., Quinn, B., Czanner, S., Busa, E., Pacheco, J., Albert, M., Killiany, R., Maguire, P., Rosas, D., Makris, N., Dale, A., Dickerson, B., Fischl, B., 2006. Reliability of MRI-derived measurements of human cerebral cortical thickness: the effects of field strength, scanner upgrade and manufacturer. Neuroimage 32 (1), 180–194.

Greve, D.N., Fischl, B., 2009. Accurate and robust brain image alignment using boundary-based registration. Neuroimage 48 (1), 63–72.

Desikan, R.S., Ségonne, F., Fischl, B., Quinn, B.T., Dickerson, B.C., Blacker, D., Buckner, R.L., Dale, A.M., Maguire, R.P., Hyman, B.T., Albert, M.S., Killiany, R.J., 2006. An automated labeling system for subdividing the human cerebral cortex on MRI scans into gyral based regions of interest. Neuroimage 31 (3), 968–980.

Liao, W., Chen, H., Yang, Q., Lei, X., 2008. Analysis of fMRI data using improved self-organizing mapping and spatio-temporal metric hierarchical clustering. IEEE Trans. Med. Imaging 27, 1472–1483 no. October.

Cheng, D., Kannan, R., Vempala, S., Wang, G., 2006. A divide-and-merge methodology for clustering. ACM Trans. Database Syst. 31 (4), 1499–1525.

Andreopoulos, B., An, A., Wang, X., Schroeder, M., 2008. A roadmap of clustering algorithms: finding a match for a biomedical application. Brief. Bioinform. 10 (3), 297–314.

Kriegel, H.P., Kröger, P., Sander, J., Zimek, A., 2011. Density-based clustering. Wiley Interdiscip. Rev. Data Min. Knowl. Discov. 1 (3), 231–240.

Rousseeuw, P.J., 1987. Silhouettes: a graphical aid to the interpretation and validation of cluster analysis. J. Comput. Appl. Math. 20, 53–65 no. C.

Bergstra, J., Bengio, Y., 2012. Random search for hyper-parameter optimization. J. Mach. Learn. Res. 13, 281–305.

Yang, J., Honavar, V., 1997. Feature subset selection using a genetic algorithm. Pattern Recognit. 13 (2), 380.

Shahamat, H., Pouyan, A.A., 2015. Feature selection using genetic algorithm for classification of schizophrenia using fMRI data. J. Artif. Intell. Data Min. 3 (1), 30–37.

Hackert, V.H., den Heijer, T., Oudkerk, M., Koudstaal, P.J., Hofman, A., Breteler, M.M., 2002. Hippocampal head size associated with verbal memory performance in nondemented elderly. Neuroimage 17 (3), 1365–1372.

Greicius, M.D., Krasnow, B., Boyett-Anderson, J.M., Eliez, S., Schatzberg, A.F., Reiss, A.L., Menon, V., 2003. Regional analysis of hippocampal activation during memory encoding and retrieval: fMRI study. Hippocampus 13 (1), 164–174.

Destrieux, C., Bourry, D., Velut, S., 2013. Surgical anatomy of the hippocampus. Neurochirurgie 59 (4–5), 149–158.

Torres, G., Basnet, R., Sung, A., 2008. A similarity measure for clustering and its applications. Proc. World Acad. Sci. Eng. Technol. 31 (1307–6884), 490–496.

Duarte, I.C., Ferreira, C., Marques, J., Castelo-Branco, M., 2014. Anterior/posterior competitive deactivation/activation dichotomy in the human hippocampus as revealed by a 3D navigation task. PLoS One 9 (1).

Prince, S.E., Daselaar, S.M., Cabeza, R., 2005. Neural correlates of relational memory: successful encoding and retrieval of semantic and perceptual associations. J. Neurosci. 25 (5), 1203–1210.

Sugar, J., Witter, M.P., van Strien, N.M., Cappaert, N.L.M., 2011. The retrosplenial cortex: intrinsic connectivity and connections with the (para)hippocampal region in the rat. An interactive connectome. Front. Neuroinform. 5, 7 no. July.

Olman, C.A., Harel, N., Feinberg, D.A., He, S., Zhang, P., Ugurbil, K., Yacoub, E., 2012. Layer-specific fmri reflects different neuronal computations at different depths in human V1. PLoS One 7 (3).

Kok, P., Bains, L.J., Van Mourik, T., Norris, D.G., De Lange, F.P., 2016. Selective activation of the deep layers of the human primary visual cortex by top-down feedback. Curr. Biol. 26 (3), 371–376.

Wolosin, S.M., Zeithamova, D., Preston, A.R., 2012. Reward modulation of hippocampal subfield activation during successful associative encoding and retrieval. J. Cogn. Neurosci. 24 (7), 1532–1547.

Ryan, L., Lin, C.Y., Ketcham, K., Nadel, L., 2010. The role of medial temporal lobe in retrieving spatial and nonspatial relations from episodic and semantic memory. Hippocampus 20 (1), 11–18.

Hirshhorn, M., Grady, C., Rosenbaum, R.S., Winocur, G., Moscovitch, M., 2012. The hippocampus is involved in mental navigation for a recently learned, but not a highly familiar environment: a longitudinal fMRI study. Hippocampus 22 (4), 842–852.

Woollett, K., Maguire, E.A., 2012. Exploring anterograde associative memory in London taxi drivers. Neuroreport 23 (15), 885–888.

Khan, R., Zhang, Q., Darayan, S., Dhandapani, S., Katyal, S., Greene, C., Bajaj, C., Ress, D., 2011. Surface-based analysis methods for high-resolution functional magnetic resonance imaging. Graph Models 73 (6), 313–322.

Jones, S.E., Buchbinder, B.R., Aharon, I., 2000. Three-dimensional mapping of cortical thickness using Laplace's equation. Hum. Brain Mapp. 11 (1), 12–32.

Waehnert, M.D., Dinse, J., Weiss, M., Streicher, M.N., Waehnert, P., Geyer, S., Turner, R., Bazin, P.L., 2014. Anatomically motivated modeling of cortical laminae. Neuroimage 93, 210–220.

Glosser, G., Saykin, A.J., Deutsch, G.K., O'Connor, M.J., 1995. Neural organization of material-specific memory functions in temporal lobe epilepsy patients as assessed by the intracarotid amobarbital test. Neuropsychology 9 (4), 449–456.
Owens, M.M., Yuan, D., Hahn, S., Albaugh, M., Allgaier, N., Chaarani, B., Potter, A., Garavan, H., 2020. Investigation of psychiatric and neuropsychological correlates of default mode network and dorsal attention network anticorrelation in children. Cereb. Cortex 30 (12), 6083–6096.
Stiernman, L.J., Grill, F., Hahn, A., Rischka, L., Lanzenberger, R., Lundmark, V.P., Riklund, K., Axelsson, J., Rieckmann, A., 2021. Dissociations between glucose metabolism and blood oxygenation in the human default mode network revealed by simultaneous PET-fMRI. Proc. Natl. Acad. Sci. USA. 118 (27) pp. e2021913118.
Wang, S.F., Ritchey, M., Libby, L.A., Ranganath, C., 2016. Functional connectivity based parcellation of the human medial temporal lobe. Neurobiol. Learn. Mem. 134, 123–134.